

2021-09-15

The extreme 2013/14 winter storms: Regional patterns in multi-annual beach recovery

Konstantinou, A

<http://hdl.handle.net/10026.1/17462>

10.1016/j.geomorph.2021.107828

Geomorphology

Elsevier BV

All content in PEARL is protected by copyright law. Author manuscripts are made available in accordance with publisher policies. Please cite only the published version using the details provided on the item record or document. In the absence of an open licence (e.g. Creative Commons), permissions for further reuse of content should be sought from the publisher or author.

The extreme 2013/14 winter storms: Regional patterns in multi-annual beach recovery

Aikaterini Konstantinou ^{1*}, Christopher Stokes ¹, Gerd Masselink ¹, Timothy Scott ¹

¹ Coastal Processes Research Group, School of Biological and Marine Sciences, University of Plymouth, Plymouth PL4 8AA, UK;

* Correspondence: a.konstantinou@plymouth.ac.uk; +44 7511 044 601

Highlights

- Post-storm recovery patterns were regionally coherent and can be grouped into four main types.
- High energy, fully exposed sites remained at a more eroded state over multiple winter seasons.
- Highly embayed sites with strong geological controls appear to be inherently resilient to storms.
- Regional monitoring programmes could focus on a limited number of strategically selected sites.

Abstract

Understanding the mechanisms and timescales required for beaches to recover from extreme storm events is fundamental for coastal management worldwide. Yet the post-storm recovery characteristics of different beach types have rarely been investigated over multi-annual timescales. Previous work along the southwest coast of England has suggested that the magnitude and alongshore variability of beach response to storms can be grouped into four key response types controlled by the level of exposure, angle of storm wave approach and degree of embaymentisation. This study aims to enhance our understanding of the spatial and temporal patterns of post-storm beach recovery within this storm response classification framework. Analysis was based on morphological survey data from 23 sites along the southwest coast of England collected between 2012 and 2017. We found that beaches that responded similarly to the unprecedented storm sequence of 2013/14, recovered in a similar manner too, and that spatio-temporal patterns of post-storm recovery can, for the most part, also be described by four coherent classes. In terms of complete recovery to pre-2013/14 volumes, 7 of the 23 beaches we studied recovered >90% of their sediment within 3 years or less, including some of the most affected sites. The magnitude of intertidal beach volume recovered (in the order of 1-100m³m⁻¹) was well correlated with the storm erosion volume ($R = -0.81$, $p = 0.00$) and, importantly, was similar for beaches within the same response class. Fully exposed, cross-shore dominated beaches experienced the highest gross erosion and recovery volumes, but showed the lowest net recovery after 3 years (median: 74% volume recovered), while semi-exposed cross-shore dominated beaches showed lower gross change, but the highest net recovery (median: 93% volume recovered). In most cases, the spatial

pattern of recovery mirrored that of the storm impact, regardless of whether the beach was cross-shore or alongshore dominant. The observed coherency within each of the four studied beach response classes indicates that regional monitoring programmes could make considerable cost savings by strategically targeting monitoring at representative sites within each class, rather than monitoring all beaches within a region.

Keywords

Beach recovery; storm response; LiDAR; beach classification; extreme storms; geomorphic change detection; coastal management.

1. Introduction

Understanding the mechanisms and timescales required for beaches to naturally recover from erosive events is a fundamental requirement for effective coastal management (Callaghan *et al.*, 2013; Phillips *et al.*, 2015). Such information also has the potential to save money where engineering solutions are sought, but natural recovery may have otherwise occurred. Beach recovery, however, is often highly non-linear and compounded by the complex interplay between atmospheric and ocean forcing, inherited geomorphological controls, and human interventions (Burningham & French, 2017). In contrast to the relatively short time-scale over which storm-driven changes occur, recovery takes place over varying and often significantly longer timescales (Brenner *et al.*, 2018), ranging from days (Coco *et al.*, 2014; Poate *et al.*, 2016), months (Wang *et al.*, 2006; Sénéchal *et al.*, 2015; Phillips *et al.*, 2017), years (Doddet *et al.*, 2019; Castelle *et al.*, 2017), and even decades (Thom & Hall, 1991; McLean *et al.*, 2010; Turner *et al.*, 2016; Burningham & French, 2017). In this context, identifying similarities in observed patterns of beach recovery between sites subjected to the same regional scale forcing, may provide essential information for coastal management applications (Bracs *et al.*, 2016), and could provide efficiencies for long-term coastal monitoring schemes.

The 2013/14 winter season was the most energetic winter experienced on the Western European seaboard since at least 1948 and left most of the coastline in its most depleted state in decades (Masselink *et al.*, 2015a). Fully exposed sites in the UK (Perranporth) and France (Truc Vert) experienced sediment losses in excess of $200 \text{ m}^3\text{m}^{-1}$ (Masselink *et al.*, 2016). Barrier overwash occurred at many sites (Blaise *et al.*, 2015) and practically all dune systems suffered substantial erosion (Blaise *et al.*, 2015; Castelle *et al.*, 2015). Storm conditions along the southwest coast of England during that winter were exceptional with wave heights in the area exceeding average by 40% and total storm duration was more than twice that of the next ranking season. Most importantly perhaps, the total number of storm days during that winter was 200% greater than the second most energetic winter

since 1948 (Masselink *et al.*, 2016). Coastal impacts in the region were severe and widespread (Masselink *et al.*, 2015a; Scott *et al.*, 2016); practically all coastal towns were affected in some way with widespread flooding and/or damage to infrastructure and coastal defences. Many beaches lost large quantities of sediment to the extent that some were completely stripped, exposing the underlying bedrock (Masselink *et al.*, 2015b; Scott *et al.*, 2016) and record wave runup heights were reported on a number of gravel beaches (Poate *et al.*, 2016). Aside from their intensity, the impacts of the 2013/14 storms in SW England were characterised by considerable spatial variability controlled by both storm-specific conditions (wave characteristics associated with storm intensity and storm track), site-specific characteristics (beach orientation and beach type), and tidal phase (Masselink *et al.*, 2015b).

Masselink *et al.* (2015b) and Scott *et al.* (2016) studied the geomorphic storm response of 38 beaches in SW England using RTK-GPS cross-shore profile data. Two broad response categories were identified, mainly controlled by beach orientation and degree of embaymentisation: (i) a cross-shore mechanism, dominant in exposed sandy beaches on the northern coast and (ii) an alongshore mechanism prevalent on the south coast and sheltered northern coast beaches with an oblique wave incidence angle. These studies revealed that cross-shore sediment transport processes, in both dissipative and reflective sandy beaches exposed to mostly shore-normal incident angles, resulted in significant erosion occurring in the supra- and inter-tidal zones and accretion in sub-tidal bar region. Similarly, exposed gravel beaches experienced overwash with significant sediment losses landward (Poate *et al.*, 2016; Scott *et al.*, 2016). Conversely, semi-sheltered beaches exposed to oblique wave forcing were dominated by alongshore sediment transport mechanisms resulting in little net change but significant sediment redistribution as a result of longshore transport (Scott *et al.* 2016; Wiggins *et al.*, 2019a).

Burvingt *et al.* (2017a) took advantage of the superior spatial resolution and coverage offered by airborne Light Detection and Ranging (LiDAR) surveys to study the regional variability in coastal response of 157 beaches in southwest England. They used hierarchical cluster analysis based on geological variables extracted from the LiDAR data set to assess the similarity between sites and determine the grouping of beaches. Response type was found to be controlled by the level of exposure and angle of storm wave approach and degree of embaymentisation. Their analysis identified four key response classes differentiated by the magnitude and longshore variability of volumetric change:

1. Class 1 beaches (CL1): **Large, alongshore uniform** response in the order of $100 \text{ m}^3\text{m}^{-1}$ (herein, $O(100 \text{ m}^3\text{m}^{-1})$). These were sites experiencing small wave incidence angles $O(10^\circ)$ and the highest cross-shore wave power $O(170 \text{ kWm}^{-1})$;

2. Class 2 beaches (CL2): **Moderate, alongshore uniform** response $O(50 \text{ m}^3\text{m}^{-1})$. These were sites experiencing slightly larger wave incidence angles $O(20^\circ)$ and lower cross-shore wave power $O(120 \text{ kWm}^{-1})$ compared to CL1 beaches;
3. Class 3 beaches (CL3): **Limited response** characterized by considerable variability in both the alongshore and cross-shore directions. Typically, these were short, sheltered beaches, subject to larger wave incidence angles $O(60^\circ)$ and lower cross-shore wave power $O(30 \text{ kWm}^{-1})$;
4. Class 4 beaches (CL4): **Rotational response** characterized by considerable, alongshore variable response with limited net changes. Typically, sheltered beaches exposed to oblique wave incidence angles $O(55^\circ)$ and the lowest cross-shore wave power $O(25 \text{ kWm}^{-1})$.

Despite the extensive literature on storm impacts (e.g., Houser & Greenwood, 2005; Suanez, *et al.*, 2010; Castelle *et al.*, 2015; Masselink *et al.*, 2015a; Beuzen *et al.*, 2019; Guisando-Pintado *et al.*, 2019; Anfuso *et al.*, 2020), the post-storm recovery of beaches and dunes has received less attention until relatively recently (Scott *et al.*, 2016; Brooks *et al.*, 2017; Castelle *et al.*, 2017; Phillips *et al.*, 2017; Brenner *et al.*, 2018; Dodet *et al.*, 2019). Typically, beach recovery is associated with mild wave conditions and long period swell waves (Komar, 1998). Such recovery conditions are not limited to summer; in fact, post-storm winter conditions have been found to primarily control the timescales for recovery along the SW coast of England (Scott *et al.*, 2016; Burvingt *et al.*, 2018). Additionally, Dodet *et al.* (2019) showed that for the most exposed sites subjected to normal wave approach (i.e., similar to CL1 and CL2 beaches), highly energetic winters can stall or even reverse the recovery process, whereas milder winters foster recovery. Meanwhile, more energetic summer wave conditions are vital for the remobilization of sediment transported far offshore during intense storms (Costas *et al.*, 2005; Scott *et al.*, 2016). Davidson *et al.* (2013) also showed that beaches recover sediment faster when waves remain energetic, albeit less steep than the (time-varying) equilibrium conditions for that site. Scott *et al.* (2016) hypothesised that for beaches dominated by a rotational response (i.e., some CL3 and all CL4 beaches), recovery would require longshore sediment transport to be mobilized in the opposite direction, therefore necessitating bi-directionality in the wave climate. Consequently, the timescale and magnitude of post-storm beach recovery are often determined by the very factors that drive storm response in the first place.

The recovery of beaches following the extraordinary 2013/14 winter season has drawn the focus of sever studies (e.g. Scott *et al.*, 2016; Burvingt *et al.*, 2017b; Castelle *et al.*, 2017; Burvingt *et al.*, 2018; Dodet *et al.*, 2019). These studies however were limited either by the number of sites included (e.g., on site by Castelle *et al.* (2017); five sites by Dodet *et al.* (2019)), the number of beach classes (e.g., only shore-normal wave approach by Burvingt *et al.* (2018)), the timeframe of recovery (e.g., one year by Scott *et al.* (2016)) and/or the availability of 3D LiDAR data over multiannual timescales (e.g.,

Burvingt *et al.*, 2017b). Importantly, none of these studies proceeded to compare and assess the recovery characteristics of different beach types over multiannual timescales.

In this paper we aim to enhance the understanding of natural post-storm recovery processes and timescales following the extreme wave conditions of the 2013/14 winter through two objectives: (i) to establish the extent and spatial patterns of recovery of 23 beaches along the SW coast of England over multiannual timescales (2014 to 2017) within the existing storm response classification framework; (ii) to investigate the progression of recovery at bi-annual temporal resolution, and the role of hydrodynamic forcing in the recovery cycle (2012 – 2018).

2. Methods

2.1. Study Area

The SW coast of England includes the northern facing coast, which is fully exposed to the prevailing westerly Atlantic storm waves, and the southern coast which ranges from sheltered to exposed depending on location and local shoreline orientation. The tidal regime is mostly macrotidal with a mean spring tidal range of 9.6 m at Bossington (the easternmost site on the north coast) (ATT, 2020a), decreasing to 5.5 m at Whitesand Bay at the western tip of Cornwall, and further to 4.4 m at Start Bay on the south coast of Dorset (ATT, 2020b). The coastline includes more than 150 mostly embayed beaches with highly varied geomorphology in terms of beach type, sediment characteristics, shoreline orientation and geology (Scott *et al.*, 2011). Typically, beaches are backed by cliffs and are often fronted or underlain by rocky platforms. Some sandy beaches are backed by active dune systems or engineering structures, whilst most gravel beaches form barrier systems and are backed by coastal lagoons and/or low-lying coastal plains (Masselink *et al.*, 2015a; Scott *et al.*, 2016). The selection of study sites included in Figure 1 and summarized in Table 1, was based on four independent criteria:

1. The grouping based on Burvingt *et al.* (2017a) classification scheme with the aim of providing an equally weighted sample of beach clusters;
2. Sampling north- and south-facing coast beaches equally where possible;
3. Beaches that do not exhibit highly localized processes/features (e.g., major engineered control structures, rivers or estuaries, etc) that reduce the relevance of the findings to other beaches globally;
4. The availability of spatially and temporally adequate data for the quantification of both the geomorphic response to the 2013/14 winter storm season and the subsequent recovery.

2.2. Quantification of beach response and recovery

Computed changes in beach sediment volume represent changes to the inter- and supra-tidal region that took place between three epochs (pre-storm: 2012; post-storm: 2014; and latest: 2017) and are based on data collected as part of the ongoing South West Coastal Monitoring Programme (<http://southwest.coastalmonitoring.org/>). To enable the comparison of temporarily consistent data for each epoch either Real Time Kinematic Global Positioning System (RTK-GPS) baseline topographic survey (BS) data collected by the Channel Coast Observatory (CCO) or airborne LiDAR data captured by the UK Environmental Agency (EA) (<http://www.channelcoast.org/>) were utilized. These data were used to construct digital elevation models (DEMs) of beach surfaces using ESRI ArcGIS v.10.6.. Subsequently, comparisons between epochs were used to quantify beach response (pre- to post-storm), subsequent recovery (post-storm to latest) and resulting overall change (pre-storm to latest) at all 23 sites.

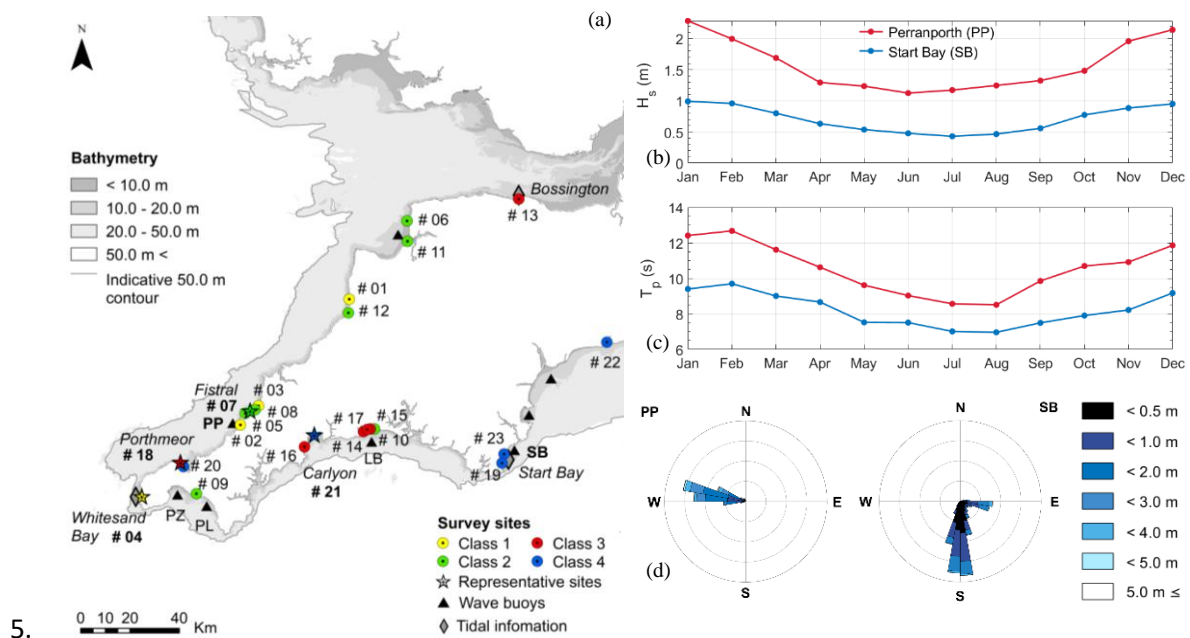


Figure 1. (a): Map of the southwest of England showing the site number and location of all study sites, as well as their classification according to Burvingt *et al.* (2017a). See Table 2 for survey site details. The locations of the nearshore directional wave buoys at Perranporth (PP), Penzance (PZ), Porthleven (PL), Looe Bay (LB), and Start Bay (SB) are also included. The four selected representative study sites that exhibit typical characteristics of each of the four distinct beach classes are indicated by a star and are further discussed in Section 2.3. (b,c): Average monthly significant wave height (b), and peak wave period (c) measured by the Perranporth (red, north coast) and the Start Bay (blue, south coast) directional wave buoys. (d): directional wave rose for Perranporth (PP) and Start Bay (SB). Measured wave data represent a 12-year record from 2007 to 2018.

The sporadic and inconsistent spatio-temporal coverage of data (Table 1) meant that data representing each epoch spread over periods ranging from 2–3 months (post-storm epoch) to over a year (pre-storm epoch). Nevertheless, seasonal topographic changes observed in the region prior to 2013/14 were

negligible compared to those that occurred during the 2013/14 winter, and spring beach volumes during 2012 and 2013 were very similar (Masselink *et al.*, 2016; Scott *et al.*, 2016). Notwithstanding these limitations, changes in beach volume derived from this dataset are considered representative of the response of beaches to, and recovery from, the winter season of 2013/14.

The beach areas were identified on high-resolution aerial photographs provided by the Plymouth Coastal Observatory (PCO) and digitized in ArcMap 10.6. To ensure consistent comparisons between DEMs, a region of interest (ROI) was defined such that it was covered by data for all three epochs. For each site, the seaward extent of the ROI typically extended from Spring Low Water Level (SLWL), while the landward extent included the active beach and dune, but excluded relatively static elements such as rocky outcrops, buildings, and cliffs. The resulting polygon shapefile defined the beach change envelope (BCE) over which all further analysis was performed. It should be stressed that only the sub-aerial and inter-tidal areas were included in this study. However, it is acknowledged that for some systems, more than one third of total sediment transport occurs in the subtidal zone (Bracs *et al.*, 2016; Valiente *et al.*, 2019b; Wiggins *et al.*, 2019a). It should therefore be noted that sediment exchange within the subtidal zone, including exchanges between adjacent subembayments, is not assessed.

Table 1. Study site characteristics and spatio-temporal structure of survey data. Site number, local name, response classification (CL1 – CL4; Burvingt *et al.*, 2017a), coast (N: north; S: south), beach orientation and length as measured and used in this study. Selected representative sites used in the detailed timeseries analysis are indicated with an asterisk. Sediment characteristics (S: sand; G: gravel) and beach type and morphology (D: dissipative; I: intermediate; R: reflective; LTBR: low tide bar/rip; NB: non-barred; LTT: low tide terrace; LTT+BR low tide terrace and bar/rip) are included where available (Scott *et al.*, 2011). Finally, survey types (BS: ground-based RTK-GPS survey; Li: airborne LiDAR survey) and month, in number format, representing each epoch are also included.

#	Site	Cl	Coast	Or.	Length (km)	Sediment type; Beach Type - Morphology	Survey type - date		
							Pre- storm (2012)	Post- storm (2014)	Latest (2017)
01	North Bude	1	N	270°	0.70	S/ -	BS-03	Li-03	BS-07
02	Perranporth	1	N	285°	3.37	S ² /D-LTBR ³	Li-03	Li-03	Li-02
03	Watergate Bay	1	N	290°	3.10	S ² /D-LTBR ³	BS-08	Li-03	BS-04
04	Whitesand Bay*	1	W	300°	1.10	S ² /I – LTT+BR	Li-02	Li-04	Li-04
05	Crantock beach	2	N	315°	0.88	S ² /D-LTBR ³	BS-06	Li-03	BS-02
06	Croyde Bay	2	N	270°	0.84	S ² / D-LTBR ³	Li-05	Li-04	Li-02
07	Fistral Beach*	2	N	300°	0.85	S ² /I-LTT+BR ³	BS-03	Li-03	BS-02
08	Newquay	2	N	330°	1.05	S ² /D	Li-04	Li-03	BS-02

09	Praa Sands	2	S	210°	1.4	S ¹ ; I - LTT+BR ³	BS-08	BS-07	BS-05
10	Seaton Beach	2	S	165°	0.70	G ¹ /I - LTT	Li-03	Li-04	Li-03
11	Westward Ho!	2	N	285°	2.18	S ² ; D - NB - D ³	Li-05	Li-04	Li-02
12	Widemouth Sand	2	N	280°	0.80	S ² ; D	BS-08	Li-03	BS-06
13	Bossington	3	N	340°	3.20	G; -	Li-05	Li-06	Li-04
14	Looe	3	S	135°	0.24	S ¹ ; I - LTT ³	Li-03	Li-04	Li-03
15	Millendreath	3	S	165°	0.16	S; -	Li-03	Li-04	Li-03
16	Pentewan Sands	3	S	120°	0.85	-; -	BS-09	Li-04	BS-01
17	Plaidy	3	S	155°	0.21	-; -	Li-03	Li-04	Li-03
18	Porthmeor*	3	N	345°	0.52	S ² ; I - LTT+BR ³	Li-04	Li-04	Li-04
19	Beesands	4	S	100°	1.50	G ¹ ; R ¹	Li-03	Li-03	Li-04
20	Carbis Bay	4	N	10°	0.90	S ² ; D - NB - D ³	Li-04	Li-04	Li-04
21	Carlyon*	4	S	170°	1.26	S ¹ ; R	Li-03	Li-04	BS-01
22	Seaton (Ax.)	4	S	180°	2.15	G ¹ ; -	BS-03	Li-05	BS-04
23	Slapton Sands	4	S	115°	5.10	G ¹ ; R - R ³	Li-03	Li-03	Li-04

¹ data obtained from Wiggins *et al.* (2019b)

² data obtained from Valiente *et al.* (2019a)

³ data obtained from Buscombe & Scott (2008)

2.2.1. Airborne LiDAR survey data

LiDAR data consist of point cloud elevation data (xyz) collected using laser scanner technology. The EA provides both pre-processed raster data (1000x1000 gridded raster tiles with 1-m resolution) and raw point cloud data (minimum point density requirement: 16 points/m²), allowing the user to apply custom filtering and interpolation in ASCII format. Many studies have shown that this level of accuracy does not compromise the value of LiDAR data for the study of coastal morphological change (Saye *et al.*, 2005; Pollard *et al.*, 2019), but as coastal environments can exhibit topographic changes of the same order, the uncertainty must be accounted for (Stockdon *et al.*, 2002; Wheaton *et al.*, 2010a; Wiggins *et al.*, 2019a), as per the method described in Section 2.2.3. Pre-processing includes the image mosaicking, filtering of spurious data, and the removal of water areas. Data is then regridded to 1-m resolution in 1-km tiles. The final LiDAR data products are delivered as unfiltered Digital Surface Model (DSM) or filtered Digital Terrain Model (DTM) in ASCII format (EA, 2015) and have a vertical measurement accuracy of ±0.15 m RMSE (Stockdon *et al.*, 2002; Middleton *et al.*, 2013; Wiggins *et al.* 2019a).

2.2.2 RTK-GPS survey data

Pole-mounted RTK-GPS baseline survey data were collected on foot with a minimum point density of 4 sample points per 5 m² (0.8 points/m²) and have a vertical measurement accuracy of ±0.03 m RMSE (Harley *et al.*, 2011; Amante, 2018). Data points were imported into ESRI ArcMap10.6 and interpolated to 1-m raster DEMs to ensure compatibility with the LiDAR data set. Areas of low sampling density and high surface complexity were excluded from the ROI to avoid localised interpolation errors. The inverse distance weighting (IDW) interpolation method was selected for this study as it has been shown to be effective in processing a large number of unevenly spaced data points and producing DEMs for coastal applications (Zhang *et al.*, 2015; Danielson *et al.*, 2016). To negate distant neighbours, IDW power was set to two and the search radius was limited to the closest 12 points. In addition, interpolation was limited to the area of interest using the BCE in order to prevent spurious interpolation outside the survey area.

2.2.3. Uncertainty analysis

When generating DEMs of difference (DoDs) for the quantification of geomorphic change, it is essential to discern the probability that observed change is real and not due to errors introduced by surveying methods or procedures (Wheaton *et al.*, 2010b). For morphological surveys, the type of instrument used for measurement, the sampling strategy, the complexity of the measured surface (primarily surface slope, curvature and roughness) and interpolation methods all contribute to the potential uncertainty of the derived DEM surface ($\delta\zeta_{DEM}$) (Heritage *et al.*, 2009; Bangen *et al.*, 2016). Assuming the horizontal components of uncertainty in vector topographic survey data (i.e., x, y, z point clouds) have a negligible influence on the derived surface differences, actual elevation (z_{act}), modelled elevation (z_{DEM}) and some measure of uncertainty ($\delta\zeta$) can be related as follows (Wheaton *et al.*, 2010a):

$$z_{DEM} = z_{act} \pm \delta\zeta, \quad (1)$$

A common approach to managing DEM errors involves specifying a spatially uniform minimum level of detection (LoD) to distinguish between actual surface changes and noise (Fuller *et al.*, 2003; Lane *et al.*, 2003; Milan *et al.*, 2011). Here, the LoD was defined based on uncertainty estimates (RMSE) for features extracted from interpolated topographic data as described in Table 2. Uncertainty in the derived DEM estimates can then be propagated into the DoD using standard linear error propagation theory combined with some measure of DEM precision derived from quality control precision estimates (e.g., standard deviation, RMSE) (Brasington *et al.*, 2000; Wheaton *et al.*, 2010b):

$$LoD = \delta\zeta_{DoD} = \sqrt{\delta\zeta_{new}^2 + \delta\zeta_{old}^2}, \quad (2)$$

where $\delta\zeta_{DoD}$ is the propagated error and $\delta\zeta_{new}$ and $\delta\zeta_{old}$ are the individual errors associated with the DEMs used to produce the DoD. Elevation differences smaller than the LoD, are excluded from further

analysis as it cannot be assumed with adequate certainty (here considered within the bounds of RMSE error) that they correspond to real change.

Table 2. Summary of survey method DEM uncertainty (RMSE) based on relevant literature and resulting DoD uncertainty (RMSE) estimated using Eq.(2)

Survey type	DEM uncertainty ($\delta\zeta$)	Reference	DoD uncertainty ($\delta\zeta_{DoD}$)
Baseline RTK-GPS	0.054 m	(Wiggins <i>et al.</i> , 2019a)	0.08 m
Airborne LiDAR	0.150 m	(Brenner <i>et al.</i> , 2018; Wiggins <i>et al.</i> , 2019a)	0.22 m
Combined LiDAR & RTK-GPS			0.16 m

2.2.4. DoD generation and volume budget estimation

Volumetric changes were computed on a cell-by-cell basis as the product of the thresholded surface elevation change and the surface area of each cell (1 m^2) and summed into erosional and accretional categories to produce the net volumetric changes within the spatial extent of the DoDs, dQ_{nt} . The gross volume change, dQ_{gr} (i.e., the sum of the absolute values of erosion and accretion), was also calculated as a measure of the total amount of sediment mobilized. Net recovery was then computed as the overall volumetric change observed over the study period (pre-storm to latest epochs) as a percentage of change during storm response phase. Volume changes were then normalised by beach longshore length, L_s , and expressed in volume change per unit beach width (dQ_N, dQ_{Ngr}) to enable comparison between sites.

To assess the longshore variability of CL4 beaches, the BCE was divided in longshore sections based on the location of pivot points revealed by the topographic data (Figure 2). Volume difference budgets were estimated for each section and phase (response, recovery, overall change).



Figure 2. Beach Change Envelope (BCE) used for alongshore budget segmentation estimations shown for: Slapton Sands (a); Beesands (b); Seaton (c); Carlyon Bay (d); and Carbis Bay (e). The profiles used for calculating beach volumes representative of the two beach extremities for Carlyon Bay are also indicated.

2.3. Temporal patterns of beach recovery and links to hydrodynamic forcing

The progression of beach recovery was investigated over the period 2014 to 2018 using bi-annual cross-shore beach profile data at four selected sites that exhibit a behaviour in response to wave forcing typical of each of the four beach types (Bracs *et al.*, 2016; Stéphan *et al.*, 2019) herein, *representative sites*. Three sites were selected on the north coast (Perranporth, CL1; Fistral, CL2; and Porthmeor, CL3), and one on the south coast (Carlyon Bay, CL4). Survey dates for each site are included in Table 3. The overall beach volume was estimated as the alongshore average profile volume between the landward and seaward extent of the BCE. The recovered sediment volume was then estimated for each autumn survey (typically between August and October) as the difference in beach volume relative to the spring 2014 (post-storm) survey.

The control of hydrodynamic forcing on beach recovery was investigated over an extended period (2012 to 2018) by comparing the biannual profile data for the four representative sites with wave forcing data. Wave forcing proxies were calculated using measured wave data obtained from nearshore Datawell Directional Waverider (DWR) Mk III buoys operated by the PCO as described in Section 2.4. Wave buoy locations are shown in Figure 1.

Table 3. Profile survey dates for the four representative beach sites. Wave buoys used for the assessment of beach forcing at each site are also included: Perranporth (PP) and Start Bay (SB).

		Profile survey dates						
	Buoy	2012	2013	2014	2015	2016	2017	2018
Perranporth	PP	Jun/Oct	Mar/Sep	Mar/Sep	Feb/Aug	Mar/Oct	Mar/Oct	Mar/Oct
Fistral	PP	Mar/Sep	Jan/Sep	Jan/Sep	Feb/Aug	Mar/Oct	Feb/Oct	Feb/Oct
Porthmeor	PP	Feb/Sep	Jan/Nov	Mar/Sep	Feb/Sep	Mar/Oct	Jan/Oct	Feb/Sep
Carlyon Bay	SB	Sep/Nov	Jun/Jul	Apr/Jul/Oct	Feb/Apr/Sep	Feb/Jan/Sep	Jan/Nov	Feb/May

2.3.1. Sites exposed to unidirectional, shore-normal hydrodynamic forcing

For sites located on the north coast and exposed to the Atlantic storm approach (CL1, CL2 and CL3), incoming wave power was normalised with respect to the long-term (2007 – 2018) average. Beach volume changes were also normalised by their range and mean to produce a volume change index (VCI) ranging from 0 (representing the most eroded state) to 1 (representing the most accreted state):

$$VCI = \frac{(dV - \overline{dV}) - (dV - \overline{dV})_{min}}{(dV - \overline{dV})_{max} - (dV - \overline{dV})_{min}}, \quad (3)$$

where dV_i are the profile-derived beach volume differences between time steps, and \overline{dV} is the mean beach volume change. Normalised wave power was then compared with the VCI to investigate the relationship between wave power and beach volumes.

2.3.2. Sites exposed to bi-directional oblique forcing

CL4 sites are exposed to two dominant wave directions and typically exhibit a rotational, response. To quantify the geomorphic change observed at such sites and assess the influence of directional wave power, the methodology proposed by Wiggins *et al.* (2019b) was adopted. Firstly, cross-shore profiles from opposing ends (east and west) of Carlyon Bay (Figure 2d) were used to calculate beach sediment volumes and establish the degree of synchronicity between the two ends of the beach. A positive correlation coefficient indicates an in-phase response, suggesting the dominance of cross-shore transport mechanisms, whereas a negative correlation coefficient indicates an out-of-phase response, suggesting an alongshore-dominated behavioural response. Finally, a rotation index (RI) was defined as the difference between the normalised volumes at the two beach ends:

$$RI = V^W - V^E \quad (4)$$

where V^W , V^E are the beach volumes calculated for the west and east sections of the beach respectively for each time step. A large positive RI indicates clockwise rotation whereas a large negative RI an anticlockwise rotation. Small RI values represent limited change and/or dominant cross-shore change.

2.4. Wave forcing analysis

Data from the Perranporth DWR buoy were used to represent the wave forcing for the three representative sites on the north coast (Fistral, Porthmeor and Perranporth). Start Bay wave buoy was used to represent wave forcing at Carlyon Bay beach, due to the similarity in exposure (Figure 1). All buoys obtain data at a 3.84 Hz frequency and record values averaged over 30-minute intervals, with a nominal accuracy of wave height and direction measurements of 3% and 1.5 degrees, respectively (Dhoop & Thompson, 2017; Dhoop & Thompson, 2019).

Instantaneous wave power (P) was calculated using Airy wave theory for random sea-states at intermediate depths with measured data (wave buoy depth range: 10–15 m) from the following relationship:

$$P = EC_g = \frac{1}{16} \rho g H_{m0}^2 Cn \quad (5)$$

where ρ and g are water density and gravitational acceleration taken as 1025 kgm^{-3} and 9.81 ms^{-1} , respectively, H_{m0} for deep/intermediate depths can be approximated by measured significant wave height (H_s) (Holthuijsen, 2007), C_g is wave group velocity, n is the group and C is wave celerity estimated for intermediate depths using the wave length approximation proposed by Fenton & McKee (1990).

For the north coast (Perranporth DWR buoy), which experiences a unidirectional wave climate, average seasonal wave power was calculated for winter (December to March) and summer (May to September) seasons and normalised by:

$$P_N = \frac{P - \bar{P}}{P_{std}} \quad (6)$$

where P , \bar{P} and P_{std} are the seasonally-averaged, long-term (2007-2018) mean, and standard deviation of wave power, respectively, each calculated separately for the winter and summer seasons. Large positive (negative) P_N represent seasonally-averaged wave conditions that are significantly higher (lower) in power than the long term average.

For the south coast where a bi-directional wave climate is dominant, the relationship between the directional wave power balance and the morphological response was explored. For this purpose, and following Wiggins *et al.* (2019b), the wave power directionality index (WDI) was computed to represent the balance between the relative contributions of the two dominant wave directions. as:

$$WDI = \frac{(P_S - P_E) - \overline{(P_S - P_E)}}{\sigma} \quad (7)$$

where $(P_S - P_E)$ is the difference between southerly and easterly directional wave power for each time interval between surveys, $\overline{(P_S - P_E)}$ is the long-term average difference and σ is the long-term standard deviation of directional power difference $(P_S - P_E)$.

The winter and summer average power of easterly waves and southerly waves was then calculated between 60° to 115° (easterly) and 115° to 240° (southerly) directions, from the Start Bay buoy. High positive WDI values would indicate the dominance of the primary directional mode (southerly), while high negative values indicate a higher proportion of the secondary directional mode (easterly). The WDI was then compared with the RI and correlations were obtained between the two. A positive correlation coefficient would indicate an in-phase response, suggesting the dominance of cross-shore transport mechanisms, whereas a negative correlation coefficient would indicate an out-of-phase response suggesting the behavioural response was alongshore dominated.

3. Results

3.1. Hydrodynamic forcing

The time series of monthly-averaged significant wave height, peak period and wave power from the Perranporth (north coast) and Start Bay (south coast) wave buoys are presented in Figure 3. Significant interannual variability and a clear seasonal signal are evident. The north coast clearly experiences more energetic conditions, particularly during the winter season (winter $H_S = 2.02$ m and $T_p = 12.1$ s; summer $H_S = 1.22$ m, $T_p = 9.2$ s) while conditions affecting the wave climate in the south coast are considerably milder (winter $H_S = 0.92$ m and $T_p = 9.1$ s; summer $H_S = 0.48$ m and $T_p = 7.3$ s). The dominant wave direction on the north coast is westerly (285°) in contrast to the south coast which experiences a bi-directional wave climate with the main direction from the southwest (150° – 210°) and the secondary component from the east (80° – 130°) (Figure 3c). The difference in wave conditions prevailing along the north and south coasts is clearly evident in Figure 3 and both the severity of the 2013/14 winter and the relative mildness of the 2016/17 winter ($H_S = 1.9$ m and $T_p = 12.0$ s) are also apparent (Figure 3). The period following the 2013/14 winter included the third (2015/16), fourth (2014/15) and sixth (2017/18) most severe winter seasons since 2007. Furthermore, the period between 2012 and 2017 also saw both the highest and lowest WDI since 2007 (1.90 in 2014 and -2.50 in 2018, respectively), suggesting considerable variability in the directional balance of easterly and southerly storms.

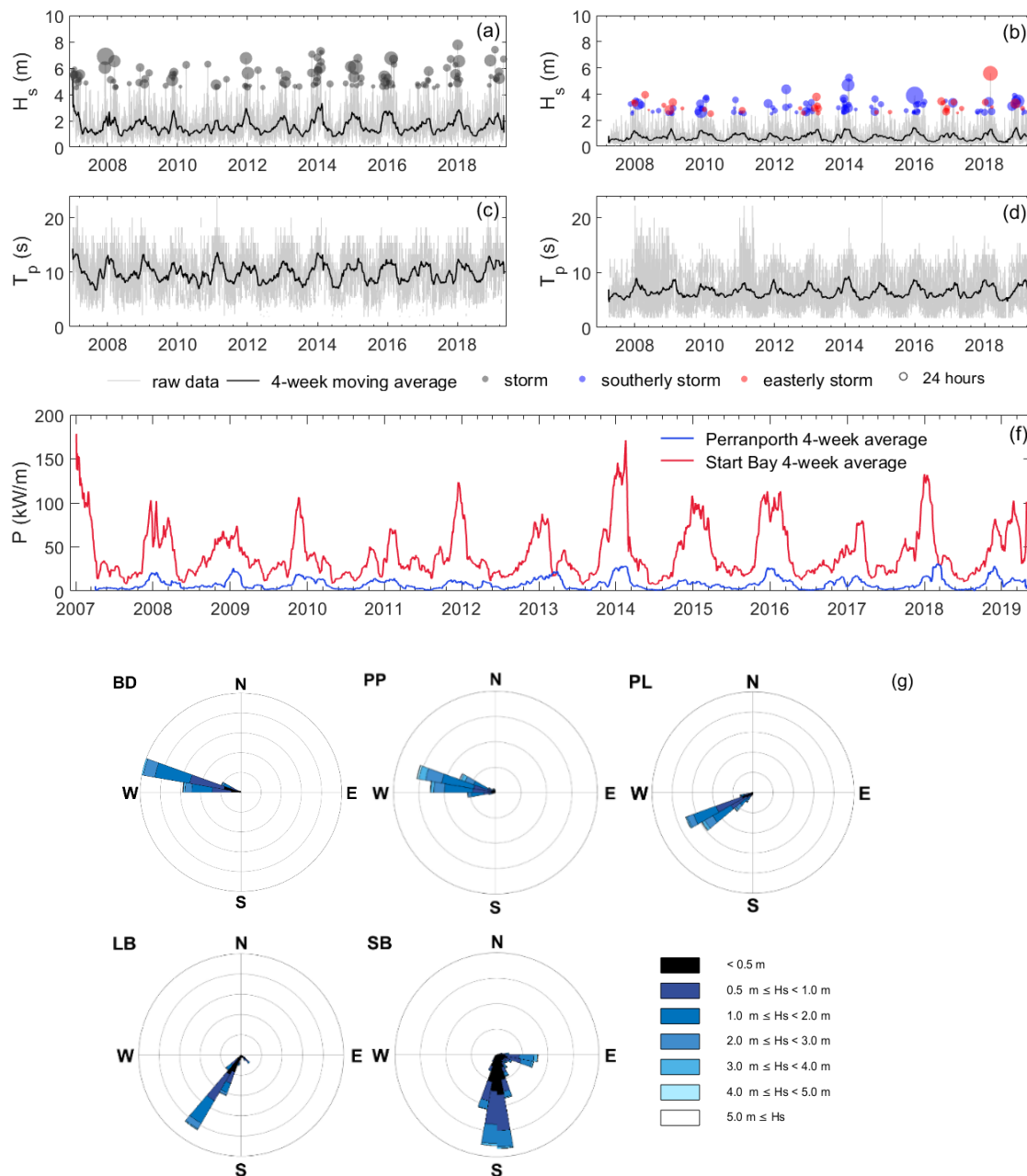


Figure 3. Wave parameter time series derived from DWR buoy measurements at Perranporth (a, c) and Start Bay (b, d) between January 2007 and December 2018: significant wave height (a, b); peak period (c, d); wave power (f). Storms (coloured circles) are identified as wave events during which H_s exceeded the 1% exceedance wave height (4.51 m at Perranporth and 2.55 m at Start Bay) and storm duration was defined as the period during which H_s remained above 5% exceedance (3.44 m and 1.76 m at Perranporth and Start Bay respectively). (g): Directional wave roses derived from the Bideford Bay (BD); Perranporth (PP); Porthleven (PL) Start Bay (SB); Bideford Bay (BD); Looe Bay (LB); and Start Bay (SB) DWR buoy data (2007-2018).

3.2. Recovery from the 2013/14 winter storm season

Typical response patterns of the four beach types are included in Figure 4. This demonstrates that the spatial pattern of recovery for CL1, CL2, and CL4 beaches closely mirrored the pattern that occurred

during the storm response epoch (Figure 4a-d). The cross-shore dominated CL1 and CL2 sites exhibited an alongshore uniform recovery pattern whereas for CL4 beaches, recovery was dominated by alongshore sediment transport resulting in rotation in the opposite direction to response. This suggests that beaches returned to an overall equilibrium planform shape during their recovery. The exception to this is CL3 beaches, where the spatial pattern of recovery did not mirror the storm response pattern. In contrast to the other beach types, response and recovery for CL3 beaches was typically spatially variable across-shore and alongshore.

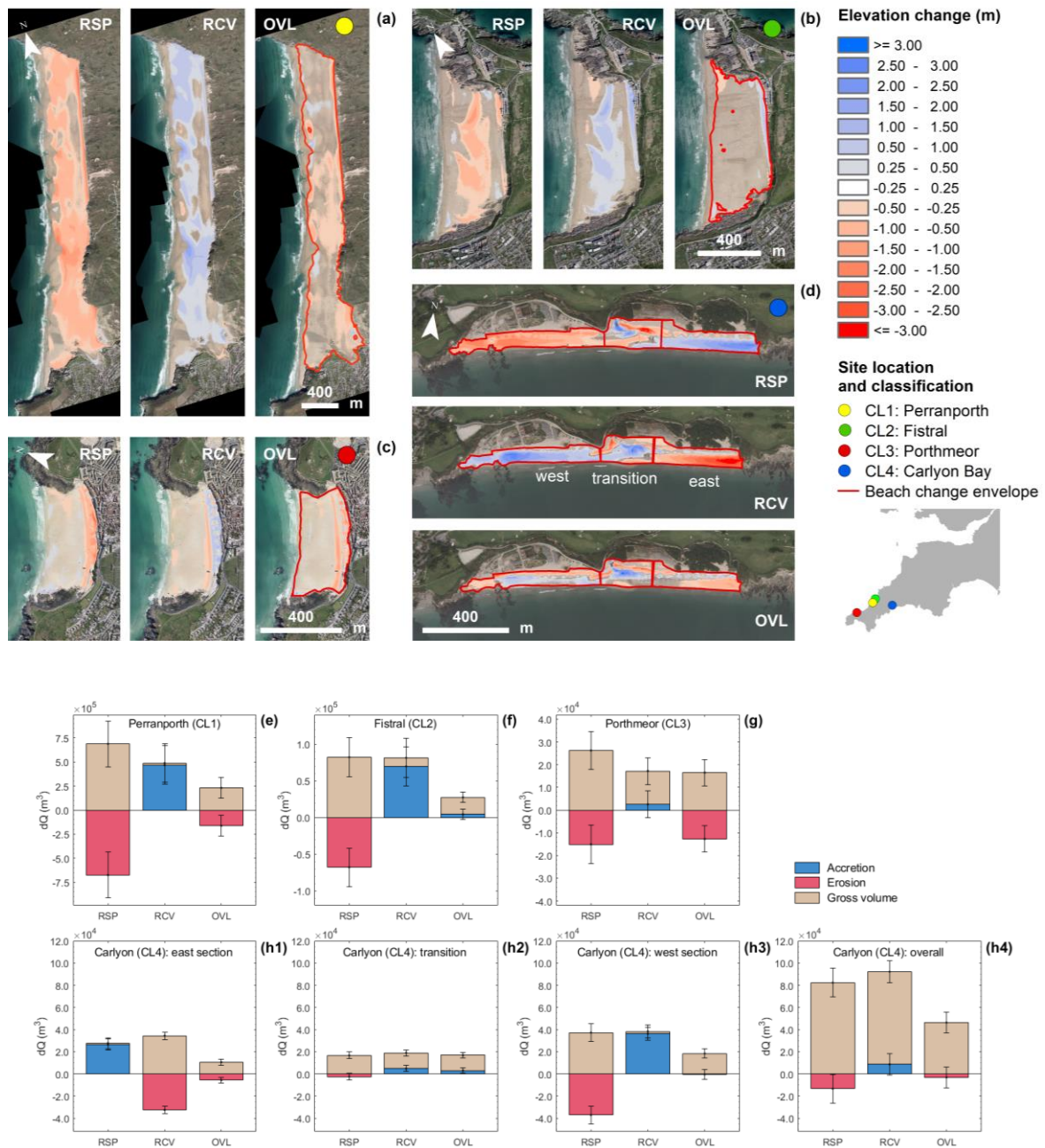


Figure 4. Examples of typical behaviour of beach clusters. Top panels: DoDs representing response (RSP), recovery (RCV) and overall (OVL) sediment volume changes for Perranporth (CL1) (a), Fistral (CL2) (b), Porthmeor (CL3) (c) and Carlyon Bay (CL4) (d). Bottom panels: corresponding total gross and net volume changes observed at Perranporth (e), Fistral (f) and Porthmeor (g). Overall changes at Carlyon Bay (CL4): east section (h1), transition (h2), west section (h3) and overall (h4).

Carlyon Bay (**h4**) as well as changes observed in the east (**h1**), transition (**h2**) and west (**h3**) sections of the beach are also included. Whiskers indicate measurement uncertainty.

Table 4. Normalised total net volume differences (dQ_N) corresponding to response (RSP), recovery (RCV) and overall (OVL) change, as well as resulting overall and annual recovery (R_C) observed over the study period at all sites.

Site			dQ_N (m ³ m ⁻¹)			R_C	
No	Cl	Site	RSP	REC	OVL	overall (%)	rate (%/yr)
01	1	North Bude	-199 ±46	132 ±38	-65 ±18	67 ±9	20±3
02	1	Perranporth	-200 ±70	139 ±60	-48 ±32	76 ±16	26±5
03	1	Watergate Bay	-110 ±32	85 ±31	-23 ±13	79 ±11	26±4
04	1	Whitesand Bay	-145 ±44	46 ±29	-101 ±40	30 ±27	10±9
05	2	Crantock beach	-70 ±44	-51 ±42	-113 ±26	-60 ±37	-21±13
06	2	Croyde Bay	-58 ±46	75 ±42	25 ±24	144 ±41	51±14
07	2	Fistral beach	-80 ±31	82 ±31	5 ±9	106 ±11	36±4
08	2	Newquay Bay	-27 ±20	25 ±17	-2 ±4	93 ±14	32±5
09	2	Praa Sands	-71 ±7	68 ±7	-3 ±6	96 ±8	34±3
10	2	Seaton beach	-31 ±14	17 ±10	-17 ±11	47 ±37	16±13
11	2	Westward Ho!	-77 ±44	55 ±37	-6 ±12	92 ±16	32±6
12	2	Widemouth	-91 ±33	67 ±28	-23 ±16	74 ±17	23±5
13	3	Bossington	-12 ±11	12 ±10	1 ±7	106 ±59	37±21
14	3	Looe	-23 ±11	19 ±10	-7 ±5	70 ±21	24±7
15	3	Millendreath	-55 ±18	37 ±17	-14 ±12	75 ±23	26±8
16	3	Pentewan Sands	-8 ±14	-5 ±16	-5 ±9	37 ±105	13±38
17	3	Plaidy	-4 ±2	2 ±1	-1 ±1	66 ±29	23±10
18	3	Porthmeor	-29 ±16	5 ±11	-24 ±11	16 ±39	5±13
19	4	Beesands	-14 ±6	-23 ±7	-37 ±9	-167 ±67	-54±22
20	4	Carbis	17 ±14	-3 ±9	13 ±13	76 ±77	25±26
21	4	Carlyon Bay	-11 ±10	7 ±8	-3 ±7	76 ±70	28±25
22	4	Seaton (Ax.)	0 ±5	2 ±5	2 ±3	663 ±806	227±276
23	4	Slapton Sands	-20 ±10	7±7	-12 ±9	37 ±46	12±15

Following the 2013/14 winter, the recovery at CL1 beaches showed large, uniformly distributed (disregarding rip channels) movements of sediment (average $dQ_N = -163 \text{ m}^3\text{m}^{-1}$) from offshore onto the inter- and supra-tidal zones (Table 4; Figure 4a), resulting in significant net accretion (average dQ_N

= $100 \text{ m}^3\text{m}^{-1}$). Over the three-year recovery period studied here, most CL1 beaches recovered almost three-quarters of their lost sediment (median $R_C = 74\%$), though one example (Whitesand Bay) recovered only 30%. CL2 beaches exhibited similar spatial patterns of recovery with more moderate, but still mostly longshore-uniform sediment movement (median $dQ_N = 61 \text{ m}^3\text{m}^{-1}$). Smaller volumes of sediment were mobilized at CL2 beaches than CL1 beaches during both storm impact and recovery phases, but interestingly, CL2 sites achieved higher overall levels of recovery (median $R_C = 93\%$) (Figure 5a). Common to both groups was a spatial recovery pattern that directly mirrored that of the storm impact, despite the impact occurring over a single winter and the recovery occurring over a three-year period.

Most CL3 beaches experienced limited overall volumetric change (median $dQ_N = -6 \text{ m}^3\text{m}^{-1}$), with modest erosion over the storm period and modest recovery over the recovery period. Gross and net volume changes were therefore low at CL3 sites. Unlike CL1 and CL2 beaches, CL3 beaches exhibited spatially non-uniform patterns of erosion and recovery (Figure 5a), with both cross-shore and alongshore variation occurring, and markedly different spatial distributions during the storm impact and recovery phases. Finally, CL4 beaches differed markedly from the other beach types in that they exhibited the smallest net changes in response to the 2013/14 winter (response range $-20 \text{ m}^3\text{m}^{-1} \leq dQ_N \leq 17 \text{ m}^3\text{m}^{-1}$; median $dQ_N = -11 \text{ m}^3\text{m}^{-1}$), but significant gross volume changes occurred at opposing ends of these alongshore dominated beaches (range $23 \text{ m}^3\text{m}^{-1} \leq dQ_{N_{gr}} \leq 141 \text{ m}^3\text{m}^{-1}$; median $dQ_{N_{gr}} = 41 \text{ m}^3\text{m}^{-1}$) (Figure 4h). Segmentation analysis of the DoDs indicates that considerable sediment exchange took place in the longshore direction, transporting sediment from one extremity of the beach to the other (Figure 5b,c). Recovery for these beaches therefore mostly constituted sediment moving in the opposite alongshore direction resulting in beach rotation (median $dQ_N = 2 \text{ m}^3\text{m}^{-1}$), but in some cases did not balance the storm induced change (e.g. Slapton Sands and Beesands, both sub-embayments of Start Bay) (Figure 5b,c). Out of the 23 sites included in this study, Crantock Beach (CL2) and Beesands (CL4) were the only two sites that continued to erode over the recovery period, losing a further $50 \pm 42 \text{ m}^3\text{m}^{-1}$ and $23 \pm 7 \text{ m}^3\text{m}^{-1}$, respectively and this will be discussed further in section 4.

The largest sediment volumes were mobilized for CL1 beaches during both storm and recovery phases (Figure 5a); yet these beaches achieved the lowest overall recovery, while most CL2 beaches returned close to pre-storm levels. In contrast, the lowest net volume changes occurred at CL4 beaches. Figures 5b,c however, demonstrate the strong rotational recovery confirming that significant sediment exchange took place between beach sections masking the level of sediment mobilization.

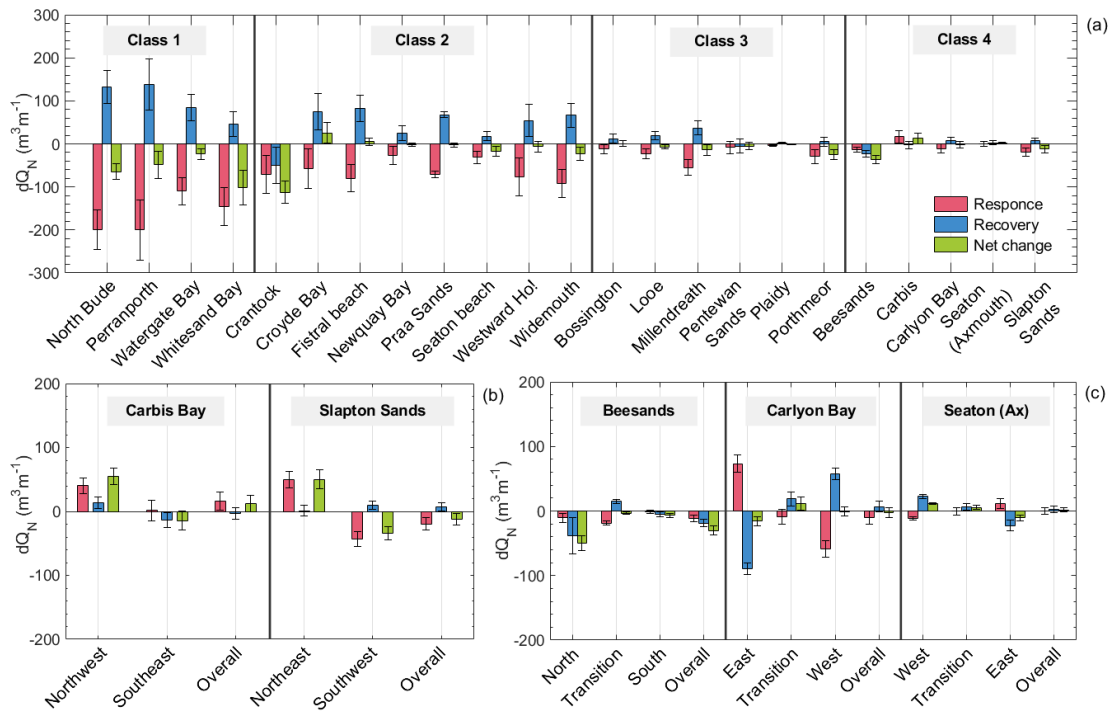


Figure 5. (a): Normalised volume changes observed in response (red) to the 2013/14 winter storms, over the recovery period (2014 to 2017; blue) and overall change (green) observed at all sites. **(b, c):** Beach volume section budgets for CL4 beaches where a two **(b)** or three-section **(c)** budget envelopes were used as shown in Figure 2.

Figure 6 further illustrates that recovery patterns and extents within clusters were mostly coherent and consistent with the storm impact classification. Furthermore, the magnitude of recovery shows a strong negative correlation with the magnitude of the storm impact – in other words, the greater the volume of sediment that was eroded from a beach, the greater the volume of sediment that returned to that beach during the subsequent recovery phase.

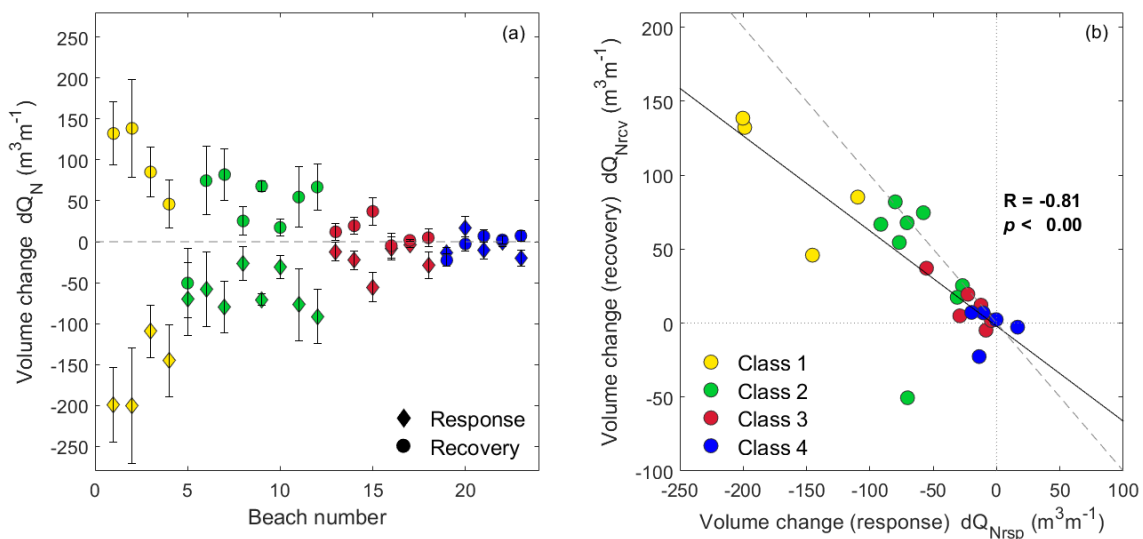


Figure 6. (a): Normalised beach volume change observed over the storm impact and recovery periods at all study sites. **(b):** Pearson correlation and linear regression of impact and recovery normalised

volumetric changes indicated a strong negative correlation. Dashed line indicates equal magnitude of volume change during storm impact and recovery. Sites to the right (left) of dashed line have resulted in net accretion (erosion).

3.3. Temporal patterns of beach evolution and control of hydrodynamic forcing

The progression of beach recovery following the 2013/14 winter and its link with hydrodynamic forcing was investigated for sites exposed to the two primary wave forcing regimes: unidirectional (CL1, CL2 and CL3) and bidirectional (CL4). Four sites exhibiting typical behaviour for each beach type were selected for this analysis: Perranporth (CL1), Fistral Beach (CL2), Porthmeor (CL3) and Carlyon Bay (CL4).

3.3.1. Sites exposed to unidirectional wave forcing

Even though the timing of the surveys was not consistent across all sites, a seasonal signal is evident in the beach volume time series at the two sites representing CL1 and CL2 (Figure 7a and 7c respectively), with erosion occurring over the winter months and accretion over the summer months. Analysis of the autumn beach volumes for each year following the 2013/14 winter (2014 – 2018) reveals an annual increase in volume at the representative CL1 and CL2 beaches (Figure 7b and 7d, respectively). By 2018, the recovery of these two sites reached 90% and 140% of the pre-2013/14 winter volumes, respectively, with average recovery rates of 20% per year ($41.1 \text{ m}^3\text{m}^{-1}/\text{yr}$) at Perranporth (CL1) and 31% per year ($33.6 \text{ m}^3\text{m}^{-1}/\text{yr}$) at Fistral (CL2). However, recovery rates showed a significant degree of non-linearity and ranged from 5% to 29% per year ($11 \text{ m}^3\text{m}^{-1}/\text{yr}$ to $60 \text{ m}^3\text{m}^{-1}/\text{yr}$) at Perranporth and from -3% to 69% per year ($-3 \text{ m}^3\text{m}^{-1}/\text{yr}$ to $74 \text{ m}^3\text{m}^{-1}/\text{yr}$) at Fistral. Examining the recovery sequence in more detail reveals that these sites recovered little sediment volume over the first summer following the 2013/14 winter (CL1: $60 \text{ m}^3\text{m}^{-1}$; CL2: $38 \text{ m}^3\text{m}^{-1}$) compared to the summer gains seen in other years. Nevertheless, compared to their pre-storm volumes, Perranporth and Fistral regained about one third of their lost sediment (29% and 35% respectively) after the first summer (2014). Notably, the impact of the following winter season (2014/15) was evidently limited at both sites (CL1: $-35.7 \text{ m}^3\text{m}^{-1}$ (-17%); CL2: $-9.6 \text{ m}^3\text{m}^{-1}$ (-9%)), even though this was one of the most energetic winters of the 12-year wave buoy record (ranked fourth). Furthermore, Fistral showed the largest relative recovery (69%) over the subsequent summer (2015) after which beach volumes returned to pre-2013/14 levels. In contrast, the 2015/16 winter (third most severe) saw both sites experiencing significant losses (CL1: $-110.3 \text{ m}^3\text{m}^{-1}$ (-54%); CL2: $-99.6 \text{ m}^3\text{m}^{-1}$ (-95%)), while relative accretion over the subsequent (2016) post-storm summer season at Perranporth and Fistral was low (5% and 12%, respectively). Though beach levels at both sites remained high (compared to pre-winter levels) over the mild 2016/17 winter, relative recovery at Fistral over the next (2017) summer was also marginal. In contrast, Perranporth regained around a fifth of its lost sediment over each of the next two

summers, (2017: 21%; 2018: 18%), despite the significant effect of the moderate 2018 winter ($-122\text{m}^3\text{m}^{-1}$ or 60%).

In contrast, Porthmeor (CL3) experienced marginal accretion ($7.0\text{ m}^3\text{m}^{-1}/\text{yr}$) rather than erosion during the 2013/14 winter and continued accreting over the first post-storm year. The beach profile time series at this site showed a weak seasonal signal and no consistent trend (Figure 7e, f) and the beach was in fact in a more eroded state before the 2013/14 winter, and post-winter 2016 and 2018, than spring 2014. However, this site also experienced significant losses over the 2015/16 severe winter and losses of the same order over the relatively milder 2017/18 winter. The storms of 2013/14, therefore, appear to have had little impact at this CL3 site, and the volumetric changes during the response and immediate recovery phase instead appear to fall within the typical variability at the site. Comparisons of normalised, seasonally-averaged wave power and the VCI parameter at the representative sites (Figure 8) indicate coherent, synchronous responses for Perranporth (CL1) and Fistral (CL2) directly linked to wave power (CL1: $R = -0.80$ CL2: $R = -0.81$; $p < 0.01$), with lower beach volumes associated with high energy seasons, and vice versa (Figure 8a,b). Conversely, at Porthmeor (CL3) there is little correlation between the volumetric state of the beach and the relative seasonal wave power (Figure 8c).

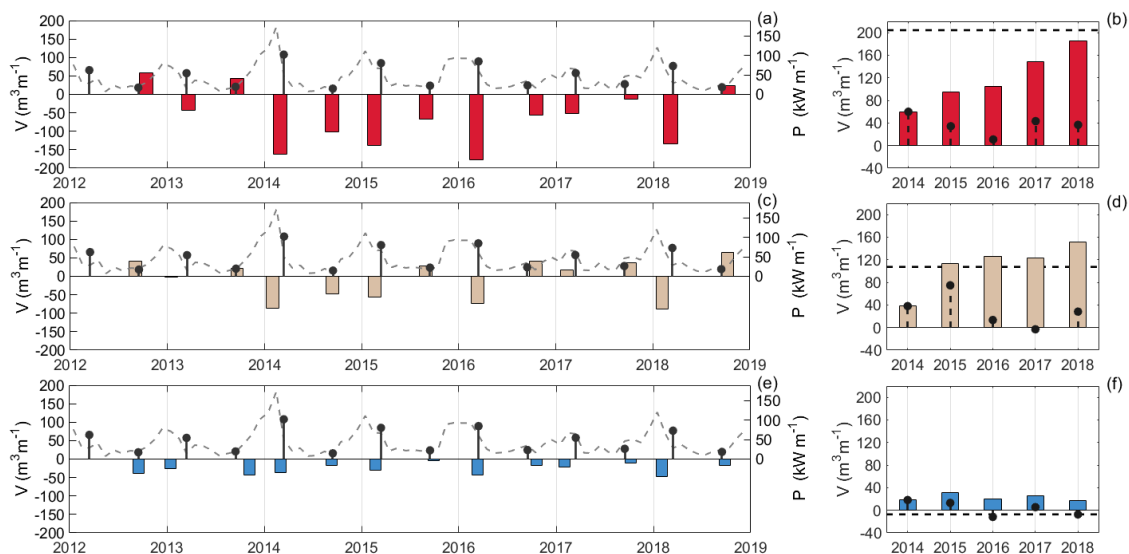


Figure 7. Beach volume time-series derived from the bi-annual RTK-GPS profile data relative to the starting volume for Perranporth (a); Fistral Beach (c) and Porthmeor (e). **Left:** Full beach volume time series (vertical bars). Dashed grey lines and black stems show monthly average and seasonal average wave power respectively, calculated from the Perranporth DWR wave buoy. **Right:** Post-storm Autumn beach volumes relative to the post 2013/14 spring beach volume, representing the cumulative recovery for Perranporth (b); Fistral Beach (d) and Porthmeor (f). Dashed lines show the pre-2013/14 beach volume, and stems represent the volume difference between consecutive autumn surveys.

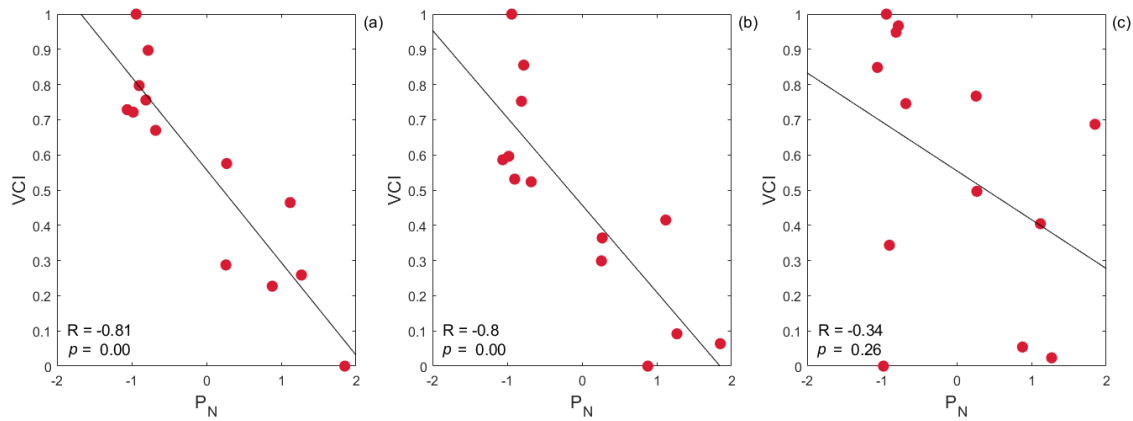


Figure 8. Pearson correlation and linear regression of the volume change index (VCI; Eq. 3) between consecutive bi-annual beach surveys and normalised wave power (P_N) for (a): Perranporth; (b): Fistral beach and (c): Porthmeor. VCI values of 0 and 1 represent the most eroded and accreted beach states, respectively, while large positive and negative values of P_N represent seasonally-averaged wave conditions that are significantly higher or lower in power than the long term average, respectively.

3.3.2. Sites exposed to bi-directional wave forcing

Analysis of the LiDAR data at Carlyon Bay (CL4) reveals rotational behaviour with limited overall volumetric change ($-19 \text{ m}^3\text{m}^{-1}$) in response to the 2013/14 storm season (Figure 4d,h). However, analysis of the RTK-GPS profile data (Figure 9b) indicates slightly lower overall sediment losses ($-13 \text{ m}^3\text{m}^{-1}$). Nevertheless, the same rotational response of the beach is captured, showing that beach volumes at the two extremities of the beach experienced significant and opposing changes over the 2013/14 winter ($67 \text{ m}^3\text{m}^{-1}$ and $-79 \text{ m}^3\text{m}^{-1}$ respectively; Figure 9d, f). Furthermore, the bi-annual volume time-series at this site (Figure 9) does not display a seasonal signal despite evident seasonality in the cumulative wave power (Figure 3b,c), indicating that wave power alone is not the primary control on beach recovery at this site. Indeed, following the 2013/14 winter, and until the end of 2016 when southerly storms prevailed (Figure 3b), the beach remained close to its post-storm state with the eastern (western) section of the beach remaining more accreted (eroded) (Figure 9c-f). However, over the next two years (end of 2016 – end of 2018) the contribution of easterly storms increased (Figure 3) and sediment was driven from the east section (Figure 9c,d) to the west section (Figure 9e,f).

Comparison of the normalised beach volume at the two ends of the beach, however, shows a clear synchronous, out of phase behaviour ($R = -0.86$, $p < 0.00$) resulting from beach rotation (Figure 10a). Furthermore, beach rotation as expressed by the rotational index RI was strongly correlated with the wave power directionality index WDI ($R = 0.76$; $p < 0.01$). This implies that recovery at this site is controlled by the balance of storm direction, and that the rotation was a result of alongshore sediment transport, rather than differences in cross-shore response at either end of the bay. In agreement with previous research (Wiggins *et al.* 2019b), these results show that a higher contribution of easterly

storms ($WDI > 0$) following 2013/14 resulted in an anticlockwise rotation ($RI > 0$) and eventual beach recovery to the pre-2013/14 configuration, whilst years with a lower contribution of easterlies ($WDI < 0$; e.g., 2013/14 winter) resulted in clockwise rotation ($RI < 0$; Figure 10b).

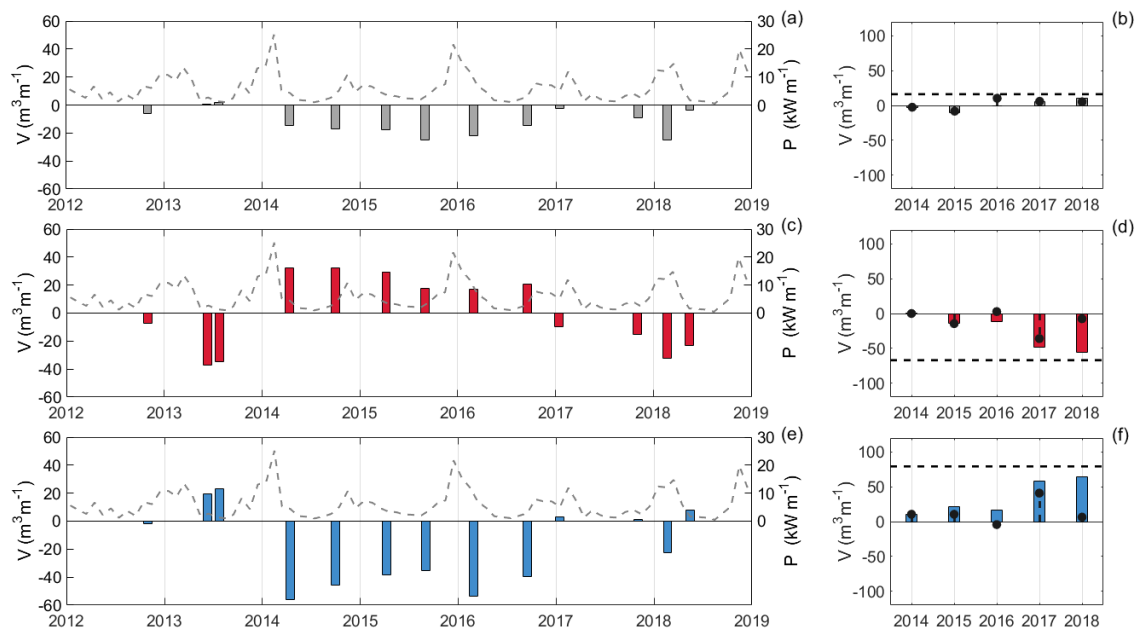


Figure 9. Left: Beach volume time series for Carlyon Bay derived from the RTK-GPS cross-shore profiles relative to the starting volume. (a): overall beach; (c): east end; (e): west end. Dashed line corresponds to cumulative monthly wave power derived from the Start Bay DWR buoy measurements. Right: Post-storm autumn beach volumes relative to response volumes (b): overall beach; (d): east end; and (f): west end. Dashed lines correspond to pre-2013/14 levels, and stem plots represent the volume difference between consecutive autumn surveys.

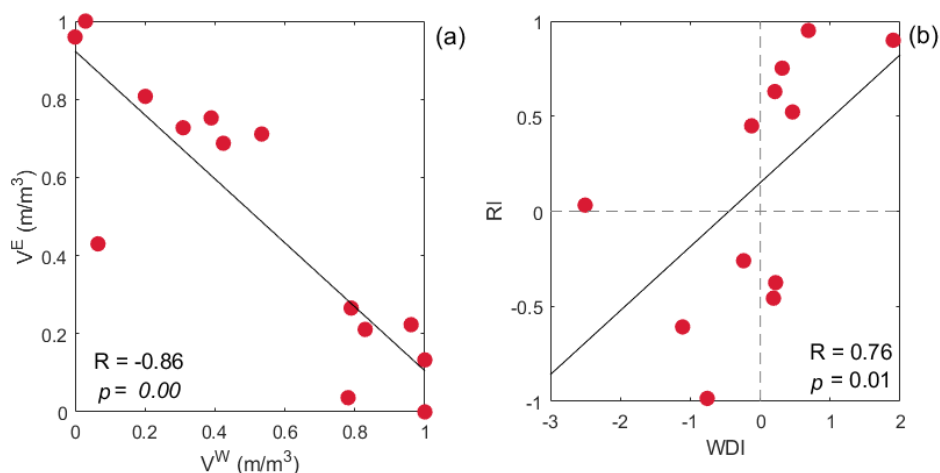


Figure 10. Pearson correlations and linear regression of morphological and forcing parameters for Carlyon Bay between: (a) normalised beach volume at the two beach extremities (V^W : west end; V^E : east end); (b) the rotational index (RI) and the wave power directionality index (WDI).

4. Discussion

An obvious finding from the present study is that beaches do not all recover from significant storm events in the same way, or at the same rate. However, it has been shown here that, despite considerable spatial variability in local wave forcing, geomorphological setting, and sediment characteristics along the coastline of SW England, beach recovery patterns can for the most part be grouped into four main classes within which recovery can be considered coherent. The beach recovery classes used here are identical to those previously used to describe coherent groupings for storm erosion impacts (Burvingt *et al.*, 2017a). Therefore, perhaps unsurprisingly, we find that beaches that respond similarly during storms, recover in a similar manner too. Furthermore, recovery volumes were found to be strongly correlated to storm erosion volumes ($R = -0.81$, $p < 0.00$); therefore, the beaches that lost the most sediment during the unprecedented winter storms of 2013/14, regained the most sediment in the subsequent 3 year recovery period, although they did not necessarily recover completely. Notably, spatial patterns of beach recovery closely mirrored the storm erosion impacts within three of the four beach response classes studied. It is therefore hypothesised that the geometry of most beaches (CL1, CL2, and CL4) tends to oscillate around an equilibrium state in relation to some long term average in the forcing conditions (Wright, Short & Green 1985; Dean, 1991; Pilkey *et al.*, 1993), regardless of whether morphological change is dominated by cross-shore (Davidson *et al.*, 2013; Splinter *et al.*, 2014) (CL1 and CL2) or alongshore (CL4) transport mechanisms (Turki *et al.*, 2013; Castelle *et al.*, 2020).

Recovery rates were markedly different between the studied beaches, though for many sites, recovery was a multi-annual process. Therefore, the characteristics of subsequent winters are important for determining the rate of recovery of these sites as well as their vulnerability to winter storms. In terms of complete recovery to pre-2013/14 volumes, almost a third (7) of the 23 studied beaches recovered more than 90% of their sediment over the 3 years following 2013/14. CL1 beaches recovered volume at a median rate of 23%/yr but none recovered fully over the study period, while CL2 beaches recovered at a significantly faster median rate of 32%/yr and most regained over 90% of their pre-2013/14 volume within 3 years or less. One example site, Fistral, regained approximately $80 \text{ m}^3\text{m}^{-1}$ (>100% recovery) within 2 years. This is somewhat remarkable, given that the wave conditions during 2013/14 represent the most energetic winter period in at least 65 years (Masselink *et al.*, 2015a). The slightly lower level of wave power and higher wave incidence angle at CL2 beaches resulted in O(50%) less sediment volume loss during 2013/14, and a significantly quicker recovery cycle than that exhibited by the CL1 sites studied. CL1 beaches, fully exposed to shore-normal high energy waves, experience a greater potential for wave-induced currents to transport sediment further offshore. Subsequent recovery of sediment retained in deeper waters then also requires relatively energetic waves to initiate onshore transport, and hence requires longer recovery timeframes (Davidson *et al.*,

2013; Scott *et al.*, 2016; McCarroll *et al.*, 2019). As already touched upon, a direct implication of the slow recovery of CL1 sites, is that they were left in a more vulnerable state, and therefore at higher risk of experiencing coastal flooding or supratidal (dune/barrier) erosion, over subsequent winter seasons.





CL4 beaches exhibited very different storm recovery characteristics to the cross-shore dominated behaviour observed at CL1 and CL2 sites. CL4 beaches experienced significantly lower net intertidal losses during 2013/14 than CL1 and CL2 sites, losing 10's of m^3m^{-1} rather than 100's m^3m^{-1} . However, the localised impact of the storms at rotational beaches was in many places an order of magnitude higher than the overall net change, due to shoreline rotation. Net recovery of overall sand volume is not, therefore, a suitable metric for beach health at CL4 sites, with most net changes nearing the measurement uncertainty. Rather than requiring accretive wave conditions for recovery as per CL1 and CL2 sites, recovery at CL4 sites occurred through opposing longshore sediment transport and rotation, which was strongly controlled by wave power directionality ($R = 0.76$; $p = 0.01$) in agreement with previous studies (Wiggins *et al.*, 2019a). However, bi-directional wave climates do not always feature a balance in wave occurrence and magnitude from either direction (Bergillos *et al.*, 2017; McCarroll *et al.*, 2019; Wiggins *et al.*, 2019a), and long-term trends or changes in weather patterns affecting the balance of alongshore wave power has resulted in chronic erosion at some CL4 sites (Scott *et al.*, 2016). To further complicate CL4 beach recovery, if waves and tides are sufficiently large during a storm, significant headland bypassing may occur (Valiente *et al.*, 2019a, 2019b). For sediment to return to a sub-embayment and re-balance beach volumes to pre-storm levels it is therefore not only necessary for a reversal in littoral drift to occur, but it must also be possible for sediment to return back around headlands bypassed in the opposite direction during the storm period. This may explain why one particular CL4 beach, Beesands, exhibited continued erosion during the recovery phase, as it is flanked on either side by headlands that allow partial bypassing to occur to other sub-embayments within Start Bay (Wiggins *et al.* 2019a).

Unlike the other three beach types, recovery of CL3 sites exhibited markedly different spatial patterns to the erosion that occurred in 2013/14 (Figure 4c), displayed varying degrees of recovery (16% to 106%), and showed little correlation between recovery and hydrodynamic forcing (Figure 8c). This suggests that sediment movement was not simply driven by cross-shore transport mechanisms (like CL1 and CL2) or alongshore mechanisms (like CL4). More likely is that these often highly embayed 'pocket' beaches experience geologically constrained sediment circulation, combining alongshore transport, headland return flows, and cross-shore transport (Goodwin *et al.* 2013; Vieira da Silva *et al.*, 2016), and so exhibit complex non-linear storm impact and recovery patterns. Importantly, gross sediment losses during the 2013/14 storms, and subsequent sediment gains during recovery, were very low ($O(1-10 \text{ m}^3\text{m}^{-1})$) at CL3 sites, with overall net volumetric change close to zero. This is likely to

be due to their low exposure to storm waves and large degree of embaymentisation minimizing storm impact and constraining nearshore sediment exchange, respectively (Masselink *et al.*, 2015b; Scott *et al.*, 2016; Burvingt *et al.*, 2017a). Therefore, despite complex sediment redistribution occurring at CL3 sites, they appear to be inherently resilient to the effects of storms.

Based on these observations, we propose a conceptual framework to describe the response and recovery characteristics of the four key beach classes differentiated by the level of wave power, angle of storm wave approach, and degree of embaymentisation (Table 5).

Table 5: Conceptual model of storm response and recovery characteristics for four key beach classes. Degree of exposure is described, including normalised beach length (NBL) defined as the ratio of alongshore length to intertidal width (Burvingt *et al.*, 2017a), and description of geological embaymentisation. Average values of cross-shore wave power and wave incidence angle experienced during the 2013/14 winter are also included. The relative magnitude and spatial variability of the storm response and recovery volume changes and order-of-magnitude yearly recovery rates for each class are also given based on the findings of the present study. The ratio net (dQ_{net}) to gross (dQ_{gross}) volume change describes the extent of redistribution of sediment within the inter- and supra-tidal area.

Typical site characteristics			Response characteristics		Recovery characteristics		
beach class	exposure/ geological control (NBL)	wave forcing (Burvingt <i>et al.</i> , 2017a)	magnitude (dQ_{net}/dQ_{gross})	spatial pattern	magnitude (dQ_{net}/dQ_{gross})	spatial pattern	recovery rate
CL1 	fully exposed/ unconstrained (4.0)	angle: O(10°) cross-shore wave power: O(170kWm ⁻¹)	Largest (>0.9)	alongshore uniform (net offshore)	largest (>0.85)	alongshore uniform (net onshore)	O(25%/yr)
CL2 	semi-exposed/ semi-constrained (3.5)	angle: O(20°) cross-shore wave power: O(120kWm ⁻¹)	moderate (0.4 to 0.9)	alongshore uniform (net offshore)	moderate (0.4 to 0.8)	alongshore uniform (net onshore)	O(33%/yr)
CL3 	Sheltered / constrained (3.5)	angle: O(60°) cross-shore wave power: O(30kWm ⁻¹)	limited (0.1 to 0.9)	variable (complex redistribution)	limited (0.1 to 0.95)	variable (complex redistribution)	variable
CL4 	Sheltered / semi- constrained (8.5)	angle: O(55°), bi-directional cross-shore wave power: O(25kWm ⁻¹)	marginal (< 0.30)	Rotation (alongshore transport)	marginal (< 0.25)	opposing rotation (alongshore transport)	variable

Understanding the geographical controls (e.g. beach orientation, influence of headlands or wider sediment cells) and hydrodynamic processes (e.g. alongshore vs cross-shore wave forcing) that drive beach recovery over different timescales is fundamental for effective coastal management (Houser *et al.*, 2015; Brenner *et al.*, 2018), and is underpinned by the collection of quantitative monitoring data (Bracks, *et al.*, 2016; Burningham & French, 2017). Given the coherency observed by Burvingt *et al.* (2017a) in storm impacts within four key beach response classes, and the similar coherency in beach recovery within those same classes identified here, we propose that response-representative beaches could be used to strategically streamline beach monitoring programs offering significant efficiency and financial savings. In essence, if the beaches in a given region can be classified into the four beach response classes (for example through an initial monitoring period of 2-3 years), subsequent monitoring would only then be required at 2-3 beaches from each class to provide a gauge of the health of all beaches in the region. This is because beaches within a given class tend to erode and recover at similar rates and with similar spatial characteristics (Figure 12). Surveying fewer beaches may also make it more feasible to capture data with consistent timing from year to year across the monitored sites, which would enhance our ability to capture long-term geomorphic change and enable robust temporal comparisons (Almeida *et al.*, 2012; Coco *et al.*, 2014; Scott *et al.*, 2016). Critically, it would free up resources to enable more responsive pre- and post-storm surveying, which is a more suitable strategy than bi-annual surveys for sites that respond over intra-annual time scales, such as CL4 beaches (Bergillos *et al.* 2017).

Naturally, some unique sites fall outside the proposed classification scheme due to location-specific processes and may still therefore require site-specific monitoring. Whitesand Bay is one such example where recovery ($R_c = 30\%$) was significantly lower than that observed at other CL1 sites (median $R_c = 76\%$). Likewise, Crantock Beach behaved differently to other CL2 sites, continuing to erode severely after 2013/14 ($R_c = -60\%$), while other CL2 beaches recovered relatively quickly (median $R_c = 93\%$). Therefore, there are beaches which do not fit with the expected recovery behaviour for the class they belong to, but in the explored cases these have been due to internal dynamics (e.g., a dramatic change in river course at Crantock) or to wider-scale transport processes (e.g., suspected divergence of sediment cells at Whitesand Bay) unique to an individual beach. Some of the variability seen in the inter-class recovery rates is likely to be due to factors such as modal beach state, sediment type, presence of dune systems or cliffs, and depth of available sediment. A full assessment of these influences was beyond the scope of the present study, but should be addressed in future work.

Although this study includes sites covering a great variety of globally encountered geomorphological settings and hydrodynamic forcing conditions, these are limited by the

prevailing characteristics in the SW of England as well as by the selection criteria we have applied. For example, sites close to tidal inlets, estuary mouths and river outflows were excluded from this study. The dynamics of these mixed energy environments become increasingly complex as their behaviour is mostly controlled by other factors such as variations in rainfall/runoff and/or anthropogenic coastal interventions (Sabatier *et al.*, 2006; Ranasinghe *et al.*, 2013; Ridderinkhof *et al.*, 2016; Lenstra *et al.*, 2019). Sites protected from incoming swell such as those in estuaries, bays or back-barrier shorelines, also show distinct behaviours that contrast those of open coast beaches (Costas *et al.*, 2005; Nordstrom and Jackson, 2012; Vila-Concejo *et al.*, 2020). Equally, sites exposed to a dominant oblique forcing leading to consistent alongshore net sediment transport directions also exhibit markedly different behaviour (Aagaard & Sørensen, 2013; Brooks *et al.*, 2017). The findings in this study are, therefore, specifically relevant to macrotidal, embayed, sandy and gravel coastlines exposed to energetic, wave-dominated forcing.

5. Conclusions

The 2013/14 winter represents the most energetic storm season in the North Atlantic in the past 65 years, leaving large sections of the western European coastline in an unprecedented state of erosion. The dramatic and devastating events of that winter, however, present a unique opportunity to study the subsequent recovery of beaches on a wide scale which until recently, has been given little attention. Whilst geographically limited, this study included sites exhibiting a wide variety of globally encountered beach characteristics (reflective to dissipative beach types, fine sand to coarse gravel, varying degrees of embaymentisation) and hydrodynamic conditions (oblique and shore normal wave incidence, high and low storm wave exposure). Thus, the findings and application of the storm response classification scheme are potentially widely applicable to different coastlines with similar geomorphology and hydrodynamic forcing. Crucially, these findings may provide useful information for coastal management applications worldwide and are particularly relevant to the cost-effective design of long-term coastal monitoring schemes.

The principal findings can be summarized as follows:

- Beaches responded to, and recovered from, storms in a coherent manner and that the magnitude and spatio-temporal patterns of post-storm recovery can, for the most part, be grouped into four main coherent classes.
- The beaches that lost the most sediment during 2013/14, regained the most sediment in the subsequent 3-year recovery period, although did not necessarily recover completely. The recovery process was thus multi-annual and only 7 of the 23 beaches we studied

recovered more than 90% of their sediment in the 3 years following 2013/14. Therefore, for many sites the characteristics of subsequent winters are important in determining recovery rates as well as beach vulnerability to winter storms.

- Beaches fully exposed to shore-normal high energy waves (CL1) displayed the highest gross volumes of both eroded and recovered sediment $O(\text{in } 100\text{'s } \text{m}^3\text{m}^{-1})$, but recovered at the slowest rate, and remained in a more vulnerable state than other beaches.
- Recovery for sites exposed to a bi-directional wave climate (CL4) is driven by a switch in the directional power balance between the two dominant directions, and any long-term changes in this balance will therefore determine to what degree such sites are able to recover in the future.
- The observed coherency within each of the four studied beach response classes indicates that regional monitoring programmes could make considerable savings by strategically targeting monitoring at a limited number of representative sites within each class, rather than monitoring all beaches within a region.

Acknowledgments: All data used in this study is provided by the Channel Coastal Observatory (<http://www.channelcoast.org/>) under Open Government License v.3. We wish to thank Olivier Burvingt for providing additional data on the classification of beach response. Discussions with Mark Wiggins and Jak McCarroll were greatly appreciated.

References

- Aagaard, T. & Sørensen, P. (2013) 'Sea level rise and the sediment budget of an eroding barrier on the Danish North Sea coast'. *Journal of coastal research*, 65 pp. 434-439. <https://doi-org.plymouth.idm.oclc.org/10.2112/SI65-074.1>.
- Almeida, L. P., Voudoukas, M. V., Ferreira, O., Rodrigues, B. A. & Matias, A. (2012) 'Thresholds for storm impacts on an exposed sandy coastal area in southern Portugal'. *Geomorphology*, 143 pp. 3-12.
- Amante, C. J. (2018) 'Estimating Coastal Digital Elevation Model Uncertainty'. *Journal of Coastal Research*, 34 (6), pp. 1382. <https://doi.org/10.2112/Jcoastres-d-17-00211.1>.
- Anfuso, G., Loureiro, C., Taaouati, M., Smyth, T. & Jackson, D. (2020) 'Spatial Variability of Beach Impact from Post-Tropical Cyclone Katia (2011) on Northern Ireland's North Coast'. *Water*, 12 (5), pp. 1380. <https://doi.org/10.3390/w12051380>.
- ATT. (2020a). Admiralty Tide Tables, Vol. 1B. Admiralty Charts and Publications: United Kingdom and Ireland.
- ATT. (2020b). Admiralty Tide Tables, Vol. 1A. Admiralty Charts and Publications: United Kingdom English Channel to River Humber.
- Bangen, S., Hensleigh, J., McHugh, P. & Wheaton, J. (2016) 'Error modeling of DEMs from topographic surveys of rivers using fuzzy inference systems'. *Water Resources Research*, 52 (2), pp. 1176-1193.

- Bergillos, R. J., Masselink, G. & Ortega-Sánchez, M. (2017) 'Coupling cross-shore and longshore sediment transport to model storm response along a mixed sand-gravel coast under varying wave directions'. *Coastal Engineering*, 129 pp. 93-104. <https://doi.org/10.1016/j.coastaleng.2017.09.009>.
- Blaise, E., Suanez, S., Stéphan, P., Fichaut, B., David, L., Cuq, V., Autret, R., Houron, J., Rouan, M., Floc'h, F., Ardhuin, F., Cancouet, R., Davidson, R., Costa, S. & Delacourt, C. (2015) Bilan des tempêtes de l'hiver 2013-2014 sur la dynamique du recul de trait de côte en Bretagne. *Geomorphologie-Relief Processus Environnement*, 21 (3), pp. 267-292. <http://dx.doi.org/10.4000/geomorphologie.11104>.
- Bracs, M. A., Turner, I. L., Splinter, K. D., Short, A. D. & Mortlock, T. R. (2016) 'Synchronised patterns of erosion and deposition observed at two beaches'. *Marine Geology*, 380 pp. 196-204. <https://doi.org/10.1016/j.margeo.2016.04.016>.
- Brasington, J., Rumsby, B. T. & McVey, R. A. (2000) 'Monitoring and modelling morphological change in a braided gravel-bed river using high resolution GPS-based survey'. *Earth Surface Processes and Landforms*, 25 (9), pp. 973-990. [https://doi.org/10.1002/1096-9837\(200008\)25:9b973::aid-esp111N3.0.co;2-y](https://doi.org/10.1002/1096-9837(200008)25:9b973::aid-esp111N3.0.co;2-y).
- Brenner, O. T., Lentz, E. E., Hapke, C. J., Henderson, R. E., Wilson, K. E. & Nelson, T. R. (2018) 'Characterizing storm response and recovery using the beach change envelope: Fire Island, New York'. *Geomorphology*, 300 pp. 189-202. <https://doi.org/10.1016/j.geomorph.2017.08.004>.
- Brooks, S. M., Spencer, T. & Christie, E. K. (2017) 'Storm impacts and shoreline recovery: Mechanisms and controls in the southern North Sea'. *Geomorphology*, 283 pp. 48-60. <https://doi.org/10.1016/j.geomorph.2017.01.007>.
- Beuzen, T., Harley, M. D., Splinter, K. D. & Turner, I. L. (2019) 'Controls of Variability in Berm and Dune Storm Erosion'. *Journal of Geophysical Research-Earth Surface*, 124 (11), pp. 2647-2665. <https://doi.org/10.1029/2019JF005184>.
- Burningham, H. & French, J. (2017) 'Understanding coastal change using shoreline trend analysis supported by cluster-based segmentation'. *Geomorphology*, 282 pp. 131-149. <https://doi.org/10.1016/j.geomorph.2016.12.029>.
- Burvingt, O., Masselink, G., Russell, P. & Scott, T. (2016) 'Beach response to consecutive extreme storms using LiDAR along the SW coast of England'. *Journal of Coastal Research*, 75 (sp1), pp. 1052-1056. <https://doi.org/10.2112/si75-211.1>.
- Burvingt, O., Masselink, G., Russell, P. & Scott, T. (2017a) 'Classification of beach response to extreme storms'. *Geomorphology*, 295 pp. 722-737. <https://doi.org/10.1016/j.geomorph.2017.07.022>.
- Burvingt, O., Masselink, G., Russell, P. & Scott, T. (2017b) 'Beach evolution and recovery from a sequence of extreme storms'. *Coastal Dynamics 2017 Proceedings*, pp. 1199-1210.
- Burvingt, O., Masselink, G., Scott, T., Davidson, M. & Russell, P. (2018) 'Climate forcing of regionally-coherent extreme storm impact and recovery on embayed beaches'. *Marine Geology*, 401 pp. 112-128. <https://doi.org/10.1016/j.margeo.2018.04.004>.
- Buscombe, D. & Scott, T. (2008) 'The Coastal Geomorphology of North Cornwall: St. Ives Head to Trevoise Head'. Plymouth, U.K.: Plymouth University.
- Callaghan, D. P., Ranasinghe, R. & Roelvink, D. (2013) 'Probabilistic estimation of storm erosion using analytical, semi-empirical, and process-based storm erosion models'. *Coastal Engineering*, 82 pp. 64-75. <https://doi.org/10.1016/j.coastaleng.2013.08.007>.
- Castelle, B., Bujan, S., Ferreira, S. & Dodet, G. (2017) 'Foredune morphological changes and beach recovery from the extreme 2013/2014 winter at a high-energy sandy coast'. *Marine Geology*, 385 pp. 41-55. <https://doi.org/10.1016/j.margeo.2016.12.006>.
- Castelle, B., Marieu, V., Bujan, S., Splinter, K. D., Robinet, A., Sénéchal, N. & Ferreira, S. (2015) 'Impact of the winter 2013-2014 series of severe Western Europe storms on a double-barred sandy coast: Beach and dune erosion

- and megacusp embayments'. *Geomorphology*, 238 pp. 135-148. <https://doi.org/10.1016/j.geomorph.2015.03.006>.
- Castelle, B., Robinet, A., Idier, D. & D'Anna, M. (2020) 'Modelling of embayed beach equilibrium planform and rotation signal'. *Geomorphology*, 369 pp. 12. <https://doi.org/10.1016/j.geomorph.2020.107367>.
- Coco, G., Sénéchal, N., Rejas, A., Bryan, K. R., Capo, S., Parisot, J. P., Brown, J. A. & MacMahan, J. H. M. (2014) 'Beach response to a sequence of extreme storms'. *Geomorphology*, 204 pp. 493-501. <https://doi.org/10.1016/j.geomorph.2013.08.028>.
- Costas, S., Alejo, I., Vila-Concejo, A. & Nombela, M. A. (2005) 'Persistence of storm-induced morphology on a modal low-energy beach: A case study from NW-Iberian Peninsula'. *Marine Geology*, 224 (1-4), pp. 43-56. Doi: <https://doi.org/10.1016/j.margeo.2005.08.003>.
- Danielson, J., Poppenga, S., Brock, J., Evans, G., Tyler, D., Gesch, D., Thatcher, C. & Barras, J. (2016) 'Topobathymetric Elevation Model Development using a New Methodology: Coastal National Elevation Database'. 76 (76), pp. 75-89. <https://doi.org/10.2112/SI76-008>.
- Davidson, M. A., Splinter, K. D. & Turner, I. L. (2013) 'A simple equilibrium model for predicting shoreline change'. *Coastal Engineering*, 73 pp. 191-202. <http://dx.doi.org/10.1016/j.coastaleng.2012.11.002>
- Dean, R. G. (1991) 'Equilibrium Beach Profiles - Characteristics and Applications'. *Journal of Coastal Research*, 7 (1), pp. 53-84. https://doi.org/10.1007/1-4020-3880-1_129
- Dhoop, T. & Thompson, C. (2017) 'Quality Assurance & Quality Control of Wave Data'. Channel Coast Observatory. National Network of Regional Coastal Monitoring Programmes of England. Southampton, U.K. Available at: https://www.channelcoast.org/ccoresources/dataqualitycontrol/QC_Manual_CCO_Waves.pdf (Accessed: 20/06/2019).
- Dhoop, T. & Thompson, C. (2019) 'Directional Waverider Metadata: Supplement for QC data download from Realtime Data page'. Channel Coast Observatory. National Network of Regional Coastal Monitoring Programmes of England. Southampton, U.K. Available at: https://www.Channelcoast.org/ccoresources/dataqualitycontrol/QC_Manual_CCO_Waves.pdf. (Accessed: 20/06/2019).
- Dodet, G., Castelle, B., Masselink, G., Scott, T., Davidson, M., Floc'h, F., Jackson, D. & Suanes, S. (2019) 'Beach recovery from extreme storm activity during the 2013–14 winter along the Atlantic coast of Europe'. *Earth Surface Processes and Landforms*, 44 (1), pp. 393-401. <https://doi.org/10.1002/esp.4500>.
- EA, 2015. 'National Network of Regional Coastal Monitoring Programs: Specification for LiDAR Surveys'. Environmental Agency, UK. Available at: <https://www.channelcoast.org/ccoresources/specificationsandbriefs/> (Accessed: 23/11/2019).
- Fenton, J. D. & McKee, W. D. (1990) 'On calculating the lengths of water waves'. *Coastal Engineering*, 14 (6), pp. 499-513. [https://doi.org/10.1016/0378-3839\(90\)90032-R](https://doi.org/10.1016/0378-3839(90)90032-R).
- Fuller, I. C., Large, A. R. G., Charlton, M. E., Heritage, G. L. & Milan, D. J. (2003) 'Reach-scale sediment transfers: an evaluation of two morphological budgeting approaches'. *Earth Surface Processes and Landforms*, 28 (8), pp. 889-903. <https://doi.org/10.1002/esp.1011>.
- Goodwin, I.D., Freeman, R., Blackmore, K., 2013. 'An insight into headland sand bypassing and wave climate variability from shoreface bathymetric change at Byron Bay, New South Wales, Australia'. *Mar. Geol.* 341:29–45. <http://dx.doi.org/10.1016/j.margeo.2013.05.005>
- Guisado-Pintado, E. & Jackson, D. W. T. (2019) 'Coastal Impact From High-Energy Events and the Importance of Concurrent Forcing Parameters: The Cases of Storm Ophelia (2017) and Storm Hector (2018) in NW Ireland'. *Frontiers in Earth Science*, 7 (190). <https://doi.org/10.3389/feart.2019.00190>.

- Harley, M. D., Turner, I. L., Short, A. D. & Ranasinghe, R. (2011) 'Assessment and integration of conventional, RTK-GPS and image-derived beach survey methods for daily to decadal coastal monitoring'. *Coastal Engineering*, 58 (2), pp. 194-205. <https://doi.org/10.1016/j.coastaleng.2010.09.006>.
- Heritage, G. L., Milan, D. J., Large, A. R. G. & Fuller, I. C. (2009) 'Influence of survey strategy and interpolation model on DEM quality'. *Geomorphology*, 112 (3-4), pp. 334-344. <https://doi.org/10.1016/j.geomorph.2009.06.024>.
- Holthuijsen, L. H. (2007) 'Waves in oceanic and coastal waters'. ed. Cambridge University, P., Cambridge: Cambridge : Cambridge University Press.
- Houser, C. & Greenwood, B. (2005) 'Profile response of a lacustrine multiple barred nearshore to a sequence of storm events'. *Geomorphology*, 69 (1-4), pp. 118-137. <https://doi.org/10.1016/j.geomorph.2004.12.005>.
- Houser, C., Wernette, P., Rentschlar, E., Jones, H., Hammond, B. & Trimble, S. (2015) 'Post-storm beach and dune recovery: Implications for barrier island resilience'. *Geomorphology*, 234 pp. 54-63. <https://doi.org/10.1016/j.geomorph.2014.12.044>.
- Komar, P. D. (1998). *Beach processes and sedimentation*. 2nd ed. Prentice-Hall, New Jersey, U.S.A. pp. 544.
- Lane, S. N., Westaway, R. M. & Hicks, M. D. (2003) 'Estimation of erosion and deposition volumes in a large, gravel-bed, braided river using synoptic remote sensing'. *Earth Surface Processes and Landforms*, 28 (3), pp. 249-271. <https://doi.org/10.1002/esp.483>.
- Lenstra, K. J. H., Pluis, S., Ridderinkhof, W., Ruessink, G. & van der Vegt, M. (2019) 'Cyclic channel-shoal dynamics at the Ameland inlet: the impact on waves, tides, and sediment transport'. *Ocean Dynamics*, 69 (4), pp. 409-425. <https://doi.org/10.1007/s10236-019-01249-3>.
- Masselink, G., Castelle, B., Scott, T., Dodet, G., Suarez, S., Jackson, D. & Floc'h, F. (2016) 'Extreme wave activity during 2013/2014 winter and morphological impacts along the Atlantic coast of Europe'. *Geophysical Research Letters*, 43 (5), pp. 2135-2143. <https://doi.org/10.1002/2015GL067492>
- Masselink, G., Scott, T., Poate, T., Russell, P., Davidson, M. & Conley, D. (2015a) 'The extreme 2013/2014 winter storms: hydrodynamic forcing and coastal response along the southwest coast of England'. *Earth Surface Processes and Landforms*, 41 (3), pp. 378-391. <https://doi.org/10.1002/esp.3836>.
- Masselink, G., Scott, T. I. M., Conley, D., Davidson, M. & Russell, P. (2015b) 'Regional variability in Atlantic storm response along the southwest coast of England', *Coastal Sediments 2015*. World Scientific. https://doi.org/10.1142/9789814689977_0260.
- McCarroll, R. J., Masselink, G., Wiggins, M., Scott, T., Billson, O., Conley, D. C. & Valiente, N. G. (2019) 'High-efficiency gravel longshore sediment transport and headland bypassing over an extreme wave event'. *Earth Surface Processes and Landforms*, 0 (ja). <https://doi.org/10.1002/esp.4692>.
- McLean, R., Shen, J. & Thom, B. (2010) 'Beach change at Bengello Beach, Eurobodalla Shire, New South Wales: 1972-2010'.
- Middleton, J. H., Cooke, C. G., Kearney, E. T., Mumford, P. J., Mole, M. A., Nippard, G. J., Rizo, C., Splinter, K. D. & Turner, I. L. (2013) 'Resolution and Accuracy of an Airborne Scanning Laser System for Beach Surveys'. *Journal of Atmospheric and Oceanic Technology*, 30 (10), pp. 2452-2464. <https://doi.org/10.1175/jtech-d-12-00174.1>.
- Milan, D. J., Heritage, G. L., Large, A. R. G. & Fuller, I. C. (2011) 'Filtering spatial error from DEMs: Implications for morphological change estimation'. *Geomorphology*, 125 (1), pp. 160-171. <https://doi.org/10.1016/j.geomorph.2010.09.012>.
- Nordstrom, K. F. & Jackson, N. L. (2012) 'Physical processes and landforms on beaches in short fetch environments in estuaries, small lakes and reservoirs: A review'. *Earth-Science Reviews*, 111 (1-2), pp. 232-247. <https://doi.org/10.1016/j.earscirev.2011.12.004>
- Phillips, M., Turner, I., Cox, R., Splinter, K. & Harley, M. (2015). 'Will the sand come back? Observations and characteristics of beach recovery'. In *Australasian Coasts & Ports Conference 2015: 22nd Australasian Coastal*

- and Ocean Engineering Conference and the 15th Australasian Port and Harbour Conference (p. 676). Engineers Australia and IPENZ.
- Phillips, M. S., Harley, M. D., Turner, I. L., Splinter, K. D. & Cox, R. J. (2017) 'Shoreline recovery on wave-dominated sandy coastlines: the role of sandbar morphodynamics and nearshore wave parameters'. *Marine Geology*, 385 pp. 146-159. <https://doi.org/10.1016/j.margeo.2017.01.005>.
- Pilkey, O. H., Young, R. S., Riggs, S. R., Smith, A. W. S., Wu, H. Y. & Pilkey, W. D. (1993) 'The Concept of Shoreface Profile of Equilibrium - A Critical Review'. *Journal of Coastal Research*, 9 (1), pp. 255-278.
- Poate, T. G., McCall, R. T. & Masselink, G. (2016) 'A new parameterisation for runup on gravel beaches'. *Coastal Engineering*, 117 pp. 176-190. <https://doi.org/10.1016/j.coastaleng.2016.08.003>.
- Pollard, J. A., Brooks, S. M. & Spencer, T. (2019) 'Harmonising topographic & remotely sensed datasets, a reference dataset for shoreline and beach change analysis'. *Scientific data*, 6 (1), pp. 42-42.
- Ranasinghe, R., Duong, T. M., Uhlenbrook, S., Roelvink, D. & Stive, M. (2013) 'Climate-change impact assessment for inlet-interrupted coastlines'. *Nature Climate Change*, 3 (1), pp. 83-87.
- Ridderinkhof, W., Hoekstra, P., Van der Vegt, M. & De Swart, H. (2016) 'Cyclic behavior of sandy shoals on the ebb-tidal deltas of the Wadden Sea'. *Continental Shelf Research*, 115 pp. 14-26. <https://doi.org/10.1016/j.csr.2015.12.014>.
- Sabatier, F., Mailliet, G., Provansal, M., Fleury, T.-J., Suanez, S. & Vella, C. (2006) 'Sediment budget of the Rhône delta shoreface since the middle of the 19th century'. *Marine Geology*, 234 (1), pp. 143-157. <https://doi.org/10.1016/j.margeo.2006.09.022>
- Saye, S. E., van Der Wal, D., Pye, K. & Blott, S. J. (2005) 'Beach-dune morphological relationships and erosion/accretion: An investigation at five sites in England and Wales using LIDAR data'. *Geomorphology*, 72 (1), pp. 128-155. <https://doi.org/10.1016/j.geomorph.2005.05.007>.
- Scott, T., Masselink, G., O'Hare, T., Saulter, A., Poate, T., Russell, P., Davidson, M. & Conley, D. (2016) 'The extreme 2013/2014 winter storms: Beach recovery along the southwest coast of England'. *Marine Geology*, 382 pp. 224-241. <https://doi.org/10.1016/j.margeo.2016.10.011>.
- Scott, T., Masselink, G. & Russell, P. (2011) 'Morphodynamic characteristics and classification of beaches in England and Wales'. *Marine Geology*, 286 (1), pp. 1-20. <https://doi.org/10.1016/j.margeo.2011.04.004>.
- Sénéchal, N., Coco, G., Castelle, B. & Marieu, V. (2015) 'Storm impact on the seasonal shoreline dynamics of a meso- to macrotidal open sandy beach (Biscarrosse, France)'. *Geomorphology*, 228 pp. 448-461. <https://doi.org/10.1016/j.geomorph.2014.09.025>.
- Splinter, K. D., Turner, I. L., Davidson, M. A., Barnard, P., Castelle, B. & Oltman-Shay, J. (2014) 'A generalized equilibrium model for predicting daily to interannual shoreline response'. *Journal of Geophysical Research-Earth Surface*, 119 (9), pp. 1936-1958. doi: <https://doi.org/10.1002/2014JF003106>.
- Stéphan, P., Blaise, E., Suanez, S., Fichaut, B., Autret, R., Floc'h, F., Cuq, V., Le Dantec, N., Ammann, J., David, L., Jaud, M. & Delacourt, C. (2019) 'Long, Medium, and Short-term Shoreline Dynamics of the Brittany Coast (Western France)'. *Journal of Coastal Research*, pp. 89-109. doi: <https://doi.org/10.2112/SI88-008.1>.
- Stockdon, H. F., Sallenger, A. H., List, J. H. & Holman, R. A. (2002) 'Estimation of shoreline position and change using airborne topographic lidar data'. *Journal of Coastal Research*, 18 (3), pp. 502-513.
- Suanez, S., S., Cariolet, J.-M. & Fichaut, B. (2010) 'Monitoring of recent morphological changes of the dune of Vougot beach (Brittany, France) using differential GPS'. *Shore and beach*, America Shore and Beach Preservation Assotiation. 78 (1), pp. 37-47. hal-00430153.
- Thom, B. G. & Hall, W. (1991) 'Behaviour of beach profiles during accretion and erosion dominated periods'. *Earth Surface Processes and Landforms*, 16 (2), pp. 113-127.

- Turki, I., Medina, R., Coco, G. & Gonzalez, M. (2013) 'An equilibrium model to predict shoreline rotation of pocket beaches'. *Marine Geology*, 346 pp. 220-232. doi:10.1002/2014JF003106.
- Turner, I. L., Harley, M. D., Short, A. D., Simmons, J. A., Bracs, M. A., Phillips, M. S. & Splinter, K. D. (2016) 'A multi-decade dataset of monthly beach profile surveys and inshore wave forcing at Narrabeen, Australia'. *Scientific Data*, 3 pp. 13. doi:10.1038/sdata.2016.24.
- Valiente, N. G., Masselink, G., Scott, T., Conley, D. & McCarroll, R. J. (2019a) 'Role of waves and tides on depth of closure and potential for headland bypassing'. *Marine Geology*, 407 pp. 60-75. <https://doi.org/10.1016/j.margeo.2018.10.009>.
- Valiente, N. G., McCarroll, R. J., Masselink, G., Scott, T. & Wiggins, M. (2019b) 'Multi-annual embayment sediment dynamics involving headland bypassing and sediment exchange across the depth of closure'. *Geomorphology*, 343 pp. 48-64. <https://doi.org/10.1016/j.geomorph.2019.06.020>.
- Vieira da Silva, G., Toldo, E.E., Klein, A.H.F., Short, A.D., Tomlinson, R., Strauss, D., 2017. A Comparison between Natural and Artificial Headland Sand Bypassing in Santa Catarina and the Gold Coast. *Australasian Coasts & Ports 2017: Working with Nature*. p. 1111.
- Vila-Concejo, A., Gallop, S. L., Largier, J. L., Jackson, D. W. T. & Short, A. D. (2020) '15 - Sandy beaches in estuaries and bays', *Sandy Beach Morphodynamics*. Elsevier, pp. 343-362. <https://doi.org/10.1016/B978-0-08-102927-5.00015-1>.
- Wang, P., Kirby, J. H., Haber, J. D., Horwitz, M. H., Knorr, P. O. & Krock, J. R. (2006) 'Morphological and Sedimentological Impacts of Hurricane Ivan and Immediate Poststorm Beach Recovery along the Northwestern Florida Barrier-Island Coasts'. *Journal of Coastal Research*, 22 (6), pp. 1382-1402. <https://doi.org/10.2112/05-0440.1>.
- Wheaton, J. M., Brasington, J., Darby, S. E., Merz, J., Pasternack, G. B., Sear, D. & Vericat, D. (2010a) 'Linking geomorphic changes to salmonid habitat at a scale relevant to fish'. *River Research and Applications*, 26 (4), pp. 469-486. <https://doi.org/10.1002/rra.1305>.
- Wheaton, J. M., Brasington, J., Darby, S. E. & Sear, D. A. (2010b) 'Accounting for uncertainty in DEMs from repeat topographic surveys: improved sediment budgets'. *Earth Surface Processes and Landforms*, 35 (2), pp. 136-156. <https://doi.org/10.1002/esp.1886>.
- Wiggins, M., Scott, T., Masselink, G., Russell, P. & McCarroll, R. J. (2019a) 'Coastal embayment rotation: Response to extreme events and climate control, using full embayment surveys'. *Geomorphology*, 327 pp. 385-403. <https://doi.org/10.1016/j.geomorph.2018.11.014>.
- Wiggins, M., Scott, T., Masselink, G., Russell, P. & Valiente, N. G. (2019b) 'Regionally-Coherent Embayment Rotation: Behavioural Response to Bi-Directional Waves and Atmospheric Forcing'. *Journal of Marine Science and Engineering*, 7 (4), pp. 18. <https://doi.org/10.3390/jmse7040116>.
- Wright, L. D., Short, A. D. & Green, M. (1985) 'Short-term changes in the morphodynamic states of beaches and surf zones: an empirical predictive model'. *Marine geology*, 62 (3-4), pp. 339-364.
- Zhang, L., Li, N., Jia, S., Wang, T. & Dong, J. (2015) 'A Method for DEM Construction Considering the Features in Intertidal Zones'. *Marine Geodesy*, 38 (2), pp. 1-13. <https://doi.org/10.1080/01490419.2014.937883>.